Local PAPR-aware precoding for OFDM based cell-free massive MIMO-OFDM systems

Rafik Zayani, Jean-Baptiste Dore, Benoit Miscopein, David Demmer

Local PAPR-aware Precoding for OFDM based Cell-Free Massive MIMO Systems

Rafik Zayani, *Member, IEEE,* Jean-Baptiste Doré, *Member, IEEE,* Benoit Miscopein, *Member, IEEE,* and David Demmer, *Member, IEEE,*

Abstract

Orthogonal frequency division multiplexing (OFDM) based Cell-free massive multiple-input multiple-output (CF-mMIMO) is the most promising combination that can provide uniformly better quality of service for users than cellular technology in sub-6GHz bands. To make OFDM based CF-mMIMO more cost-effective and more power-efficient, the access points (APs) should be implemented by using low-cost and low-quality transceiver hardware. However, transmitting OFDM signals with high peak-to-average power ratio (PAPR) via such hardware causes severe hardware impairments (HWI), damaging the system performance. Moreover, the PAPR reduction in CF-mMIMO-OFDM has never been studied in the open literature. In this paper, we present a smart and original PAPR reduction technique, referred to as *local*PAPR*free* adequate for cell-free architecture. Interestingly, the proposed technique can be implemented in a distributed and scalable fashion, achieving benefits of CF-mMIMO-OFDM. Specifically, the PAPR reduction scheme is formulated as a simple convex optimization problem solved via an efficient and steepest iterative method. In addition, we present a theoretical study to analyze the downlink (DL) spectral-efficiency (SE) and energy-efficiency (EE) performance of CF-mMIMO-OFDM under power amplifier (PA) non-linearity. In an original way, we derive closed-form expressions for the DL SE and EE for the *local* full-pilot zero-forcing (FZF) precoding scheme with large-scale fading over independent Rayleigh block fading channels while taking into account channel estimation errors and pilot contamination. This analysis can provide important insights into the practical impact of power-efficient PA. Numerical results show that the proposed *local*PAPR*free* algorithm offers excellent PAPR reduction performance while guaranteeing high transmission quality.

Index Terms

Cell-free massive MIMO, Precoding schemes, OFDM, Hardware impairment, Power amplifier, PAPR reduction, Spectral-efficiency, Energy-efficiency.

I. Introduction

During the last decades, the exponential growth in mobile data traffic has been enabled by the densification of the network infrastructure, which can be ensured by (i) increasing the cell density known as ultra-dense network (UDN) [1][2] and/or (ii) the adoption of a large number of active antennas per access point (AP), referred to as massive MIMO (mMIMO) [3][4]. Nevertheless, both cell densification and mMIMO have fundamental limitations,

R. Zayani is with ...

... are with Anonymous University.

caused by the inter-cell interference and large quality-of-service variations, making them unable to cope with the challenges of the next/sixth generation (6G) networks in terms of increasing the user-experienced data rates. Moreover, 6G is expected to drive the future of the Industry 4.0, where private/industrial networks, applications with rapid deployment of wireless access infrastructure and low power consumption are the prominent subset.

Towards this end, a revolutionary wireless technology has recently retained substantial attention in literature [5] that exploits the best aspects of ultra-dense cellular networks and the cellular mMIMO technology to overcome their aforementioned drawbacks, known as cell-free massive MIMO (CF-mMIMO). The main propriety of the CF-mMIMO technology is that there are many geographically distributed APs, but the coverage area is not divided into disjoint cells. Note that early embodiment include the popular concept of "network MIMO" [6], "distributed antenna systems (DAS)" [7] and "distributed wireless communication systems" [8], known to the third generation partnership project (3GPP) as "coordinated multi-point (CoMP)" [9]. We can distinguish CF-mMIMO from the other early technologies by two main factors which are (i) the operating regime with more APs than UEs together with the PHY operation inspired by the recent advancement in the mMIMO field and (ii) every UE is served by all the surrounding APs, stressing the cell-free aspect.

The original version of the CF-mMIMO technology was unscalable, i.e., the front-haul capacity and the computational complexity grow exponentially with the number of UEs. This is caused by the fact that all APs are connected to a central processing unit (CPU) which is responsible to coordinate and process the signals of all UEs. Very recently, a new scalable version of the CF-mMIMO was introduced, in [10], where fully distributed processing is adopted. In [11] and [12], authors introduced new scalable precoding and combining schemes together with channel estimation, power allocation, AP clustering methods, achieving very good benefits of CF-mMIMO.

On the other hand, broadband wireless channels encounter, however, large delay spread, causing frequency-selective fading in sub-6GHz bands. Encoding digital symbols on multiple orthogonal subcarriers is the best way to deal with frequency-selective channels. Here we talk about the adoption of the well-known orthogonal frequency-division multiplexing (OFDM) scheme. Therefore, in this investigation, we combine OFDM and the scalable version of CF-mMIMO, representing a very promising combination to satisfy the ever growing demands for higher data traffic and link readability.

However, CF-mMIMO-OFDM systems carry high peak-to-average power ratio (PAPR) to transmit signals. Moreover, CF-mMIMO-OFDM can be commercially viable, only when APs are deployed using power-efficient and inexpensive hardware. Consequently, high PAPR and energy-efficient hardware results in severe hardware impairments (HWIs), which is dominated by the non-linearity of the radio frequency (RF) power amplifiers (PAs). Then, major degradation in the transmission quality is occurred and CF-mMIMO-OFDM loses rapidly all its potential benefits. Therefore, it is of paramount importance to reduce the PAPR of OFDM based CF-mMIMO systems to enable cost- and energy-efficient AP deployments.

A. Related works

The PAPR reduction problem has been now studied for a long time, the first method proposed for single-input single-output (SISO)-OFDM was in 1999 [13]. Then, some enhanced methods have been introduced to improve the

power-efficiency, such as tone reservation (TR) [14], selective mapping (SLM) [15], partial transmit sequence (PTS) [16], active constellation extension (ACE) [17], coding [18] and iterative clipping and filtering [19]. These methods, which have been proposed for SISO-OFDM and classical MIMO-OFDM, can, unfortunately, provide moderate PAPR reduction that does not satisfy the requirements in highly power-efficiency for massive MIMO based 6G networks. Moreover, the bottlenecks of these methods is related to their respective drawbacks like increase of the average power (i.e., signal-to-noise ratio gap), loss in SE due to the reservation of some subcarriers, high computational complexity and high latency. That is why they do not adequate with OFDM based massive MIMO systems.

In this regard, more interesting techniques have been proposed for co-located massive MIMO-OFDM systems, like fast truncation (FITRA) algorithm [20], approximate passing (AMP)-based Bayesian method (EM-TGM-GAMP) [21] and perturbation assisted based alternative direction method of multipliers (ADMM) technique [22]. More recently, joint MU precoding and PAPR reduction schemes have been studied in [23][24], referred to as MU-PP-GDm, RZF-OPNS, POLY-POLY-Horner and POLY-OPNS. They consist in gradient-iterative method-based linear precoding. Unfortunately, all of these techniques were limited to traditional/co-located massive MIMO systems. Indeed, in this latter, a high-dimensional degrees of freedom (DoFs) are offered by equipping the base station (BS) with a large number of antennas compared to the number of served users. Interestingly, these DoFs can be exploited to effectively reduce the PAPR. In centralized CF-mMIMO, i.e., adopting high capacity front-haul connections to transfer data between the APs and the CPU, it would be possible to re-use the aforementioned techniques already proposed for co-localised mMIMO. However, their provided gain in terms of energy-efficiency will be in the cost of heavy front-hauling load, leading to reduced global system energy-efficiency. In this regard, this paper aims to propose new PAPR reduction method that is performed locally at each AP, with no instantaneous information sharing (e.g. CSI), leading to a reduced front-hauling overhead. Here, we use *local* PAPR reduction technique to stress the local nature of the proposed strategy, which is primordial to ensure the CF-mMIMO-OFDM system scalability.

B. Motivation

The development of fully distributed and scalable precoding [11] and combining [25] schemes have been carried out for, respectively, DL and UL CF-mMIMO, representing extremely interesting SE performance. In this paper, we introduce new PAPR-aware precoding scheme adapted to CF-mMIMO-OFDM. Interestingly, the proposed method can be implemented in a fully distributed and scalable manner and hence do not need any instantaneous CSI exchange via the front-haul links. Moreover, it provides a good balance between PAPR reduction and maintaining good transmission quality.

Indeed, the motivation behind this work is related to the following observations: 1) CF-mMIMO is a fresh research topic: a number of issues need to be tackled before rolling out it into practice; one of the most challenging issue is the HWI mitigation. 2) CF-mMIMO can be economically attractive only if its implementation is based on low-cost hardware, which are more subject to HWIs. To the best of our knowledge, there is no prior work investigating the PAPR reduction in emerging OFDM based CF-mMIMO systems. 3) *Local* PAPR reduction together with the latest advancements of *local* precoding schemes [11] can offer radical performance improvements, leading to practical

and energy-efficient CF-mMIMO-OFDM. 4) There is a high demand of green signal processing solutions due to concerns over making the telecommunication sector sustainable and, correspondingly, decreasing carbon dioxide (CO2) emissions, resulting in power saving and reduced environmental pollution.

C. Contributions

The main technical contributions of this paper are as follows:

- We analyze the DL SE of OFDM based CF-mMIMO running under frequency-selective channels and nonlinear power amplifiers. Contrary to works [26][27] that only apply conjugate beamforming/matched filter, we consider local precoding schemes like *local* full-pilot zero-forcing (FZF) and *local* regularized zero-forcing (RZF) studied in [11].
- We derive analytical expressions for an achievable DL SE in CF-mmIMO-OFDM under PA nonlinearity and the assumption of independent Rayleigh fading, contrary to the work in [28] that focuses only on UL CF-mMIMO. Unlike to [27], these expressions take into consideration channel estimation errors and pilot contamination.
- We develop a new algorithm, referred to as *local*PAPR*free* to efficiently reduce the PAPR of the transmit OFDM signals in scalable CF-mMIMO-OFDM. To the best of our knowledge, it is the first solution proposed, in the open literature, that can be implemented in a fully distributed and scalable manner. Moreover, we analyze the DL SE of the considered system taking into account the PAPR reduction. This analysis explicitly reveals how PA impairments at the APs affect the SE and provide important insights into the practical deployment of CF-mMIMO systems while considering real PA models.
- We investigate the energy efficiency of our considered system with and without PAPR reduction. We consider the front-haul power consumption and the consumption of real power amplifiers operated with different input power levels.

The remainder of this paper is organized as follows. In Section II, we present the OFDM based CF-mMIMO system model. We derive the DL SE and EE in Section III. The proposed algorithm is discussed in Section IV. In Section V, numerical results and discussions are provided. Finally, the conclusion and some perspectives are given in Section VI.

D. Notations

The notations used in this paper are listed as follows:

- Lowercase boldface letters (e.g. $\mathbf{x}$) stand for column vectors,
- Bold lowercase letters with a superscript $(.)^t$ (e.g. $\mathbf{x}^t$) denotes row vectors,
- Bold uppercase letters (e.g. $\mathbf{X}$) denotes matrices,
- The $\breve{}$ marks time-domain variables over the paper,
- We denote by matrix transpose, matrix conjugate transpose, matrix pseudo-inverse and trace of a matrix by $\mathbf{X}^T$,$\mathbf{X}^H$, $\mathbf{X}^\dagger$ and $tr(\mathbf{X})$, respectively,
- For a $M \times N$-dimensional matrix $\mathbf{X} = \{x_{mn}\}$,

- We use $\mathbf{x}_n$ to designate the n-th column, and $\mathbf{x}_m^t$ to designate the m-th row,
- The $N \times N$ identity matrix and the $M \times N$ all-zeros matrix are denoted by $\mathbf{I}_N$ and $\mathbf{0}_{M\times N}$, respectively,
- We use $\|\mathbf{x}\|_2$ and $\|\mathbf{x}\|_\infty$ to denote l_2-norm and l_∞-norm of vector $\mathbf{x}$, respectively,
- $\mathbf{X} = diag\{x_1, ..., x_K\}$ denotes a diagonal matrix with elements $\{x_i\}$,
- the cardinality and complement of set Ξ is $|\Xi|$ and Ξ^c, respectively,
- $\mathrm{E}[.]$ stands for the expectation operator and j denotes $\sqrt{-1}$.

II. OFDM BASED CELL-FREE MASSIVE MIMO

A. System Model

We study an OFDM based cell-free massive MIMO downlink system operating in time division duplex (TDD) mode. Let there be L APs, each equipped with M antennas, serving coherently K single-antenna users, where $LM \gg K$. We assume that all the users and the APs are randomly located in a geographic area, as shown by Fig. 1. Here, an OFDM modulator is implemented at each antenna branch and all the APs are connected through an unlimited front-haul network to central processing unit (CPU). Besides, broadband communications are considered, suffering from severe frequency selectivity. Then, the small-scale fading is considered to be frequency-selective and modeled as a tap delay line with T taps. Then, the time-domain channel response between the l-th AP and the k-th UE, $\breve{\mathbf{H}}_{l,k} \in \mathbb{C}^{M\times T}$, is given by

$$\breve{\mathbf{H}}_{l,k} = \left[\breve{\mathbf{h}}_{l,k,0}, ..., \breve{\mathbf{h}}_{l,k,T-1}\right] \tag{1}$$

and $\breve{\mathbf{h}}_{l,k,t}$ can be written as $\sqrt{\beta_{l,k}}\breve{\mathbf{g}}_{l,k,t}$, where $\beta_{l,k}$ denotes large-scale fading (i.e., variance of the channel), which is frequency and antenna independent and $\breve{\mathbf{g}}_{l,k,t} \in \mathbb{C}^{M\times 1}$, $t = 0, ..., T-1$, have i.i.d. circularly symmetric Gaussian distributed entries with zero mean and unit variance.

We denote by $\mathbf{h}_{l,k,n} \in \mathbb{C}^{M\times 1}$ its equivalent frequency-domain channel response on the n-th subcarrier, where $n = 0, ..., N-1$ and N denotes the total number of OFDM subcarriers.

Note that we consider a block-fading channel, which is constant during a time-frequency interval, known as the *coherence interval*, and varies independently between coherence intervals. Besides, we assume that the large-scale fading coefficients vary slowly, so it is constant over many coherence intervals. Then, they are assumed to be known at each AP and they are used afterwards to estimate the frequency-domain channel responses.

B. Communication Process and Impairment Model

The TDD mode separates the downlink (DL) and uplink (UL) transmissions (see Fig. 2) with the assumption of perfect channel reciprocity which can be assured by accurate calibration methods [29]. Moreover, the transmission of a TDD frame in OFDM based CF-mMIMO is performed within the coherence interval and the physical resource block (RB) width is smaller than the coherence bandwidth.

To be compliant with the 5G NR standard, let us consider a radio frame whose time-frequency resource is divided into N_{rb} resource blocks. Each RB comprises $N_{sc} = N/N_{rb}$ consecutive subcarriers. We note by $(t, n)_{l,m}$ the resource unit (RU), which represents the smallest time-frequency resource of the n-th subcarrier of the t-th OFDM symbol corresponding to the m-th antenna of the l-th AP.

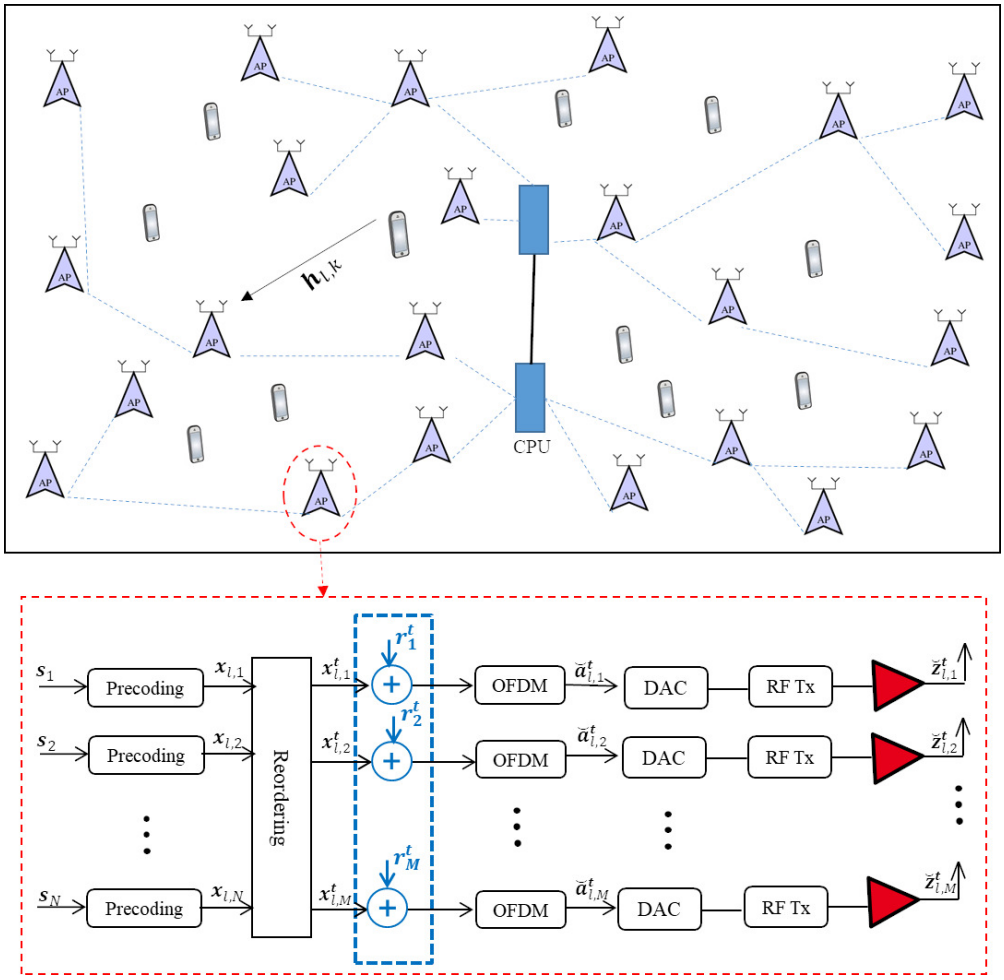

Fig. 1. System model of the OFDM based CF-mMIMO downlink: M transmit antennas at the AP, K independent single-antenna terminals, N OFDM subcarriers. The proposed PAPR reduction algorithm, highlighted by the dashed box in blue, applied independently at each AP.

Here, the TDD frame contains N_c OFDM symbols that fits the shortest coherence interval of all the users. It corresponds to the transmission of $N_{sc}N_c$ RUs per RB, where τ_p of them are used as pilots which are distributed among the UL payload transmission, as shown by Fig. 2. These pilot data will serve to estimate MK frequency-domain channels, per RB, at each AP. Consequently, we leave $N_D = N_{sc}N_c - \tau_p$ for payload data, in samples per RB, that will be split between DL and UL transmissions as ξN_D and $(1-\xi)N_D$, respectively, where $0 < \xi < 1$.

1) Uplink Training and Channel Estimation: In this investigation, we adopt a block fading channel and we assume that the frequency-domain channel coefficients for all RUs within one RB is identical and none within different RBs. Consequently, a per-RB channel estimation has to be performed.

Therefore, we consider τ_p mutually orthogonal τ_p-length frequency-domain sequences transmitted by using the first time-domain OFDM symbols (see Fig. 2), i.e., all the UEs synchronously transmit their pilot sequences to the APs, once per coherence interval. The case of practical interest is a dense network with $K > \tau_p$ so that some UEs share the same pilot, per-RB, leading to pilot contamination [30], where APs are not able to spatially

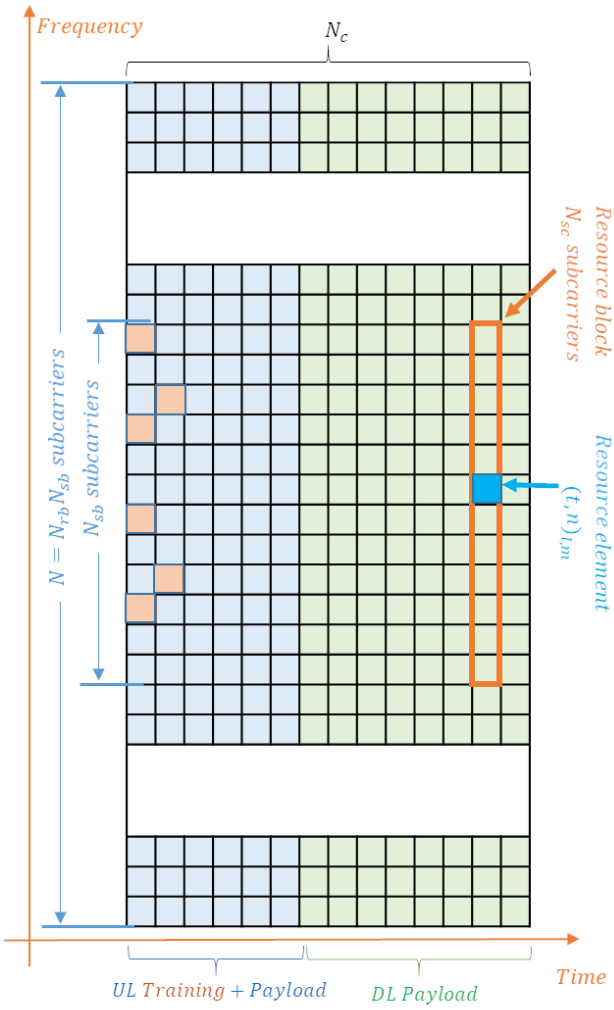

Fig. 2. A radio frame with N_c time-domain OFDM symbols and N subcarriers in frequency-domain that are grouped into N_{rb} RBs. The time-frequency resource grid of a single RB with N_{sb} subcarriers is shown. The UL training, UL payload and DL payload are also shown.

separate linearly dependent channels. For the sake of simplicity and without loss of generality, we assume that all the considered RBs are allocated to all served UEs.

Let $\theta_{i_k} \in \mathbb{C}^{\tau_p \times 1}$ is the frequency-domain pilot sequence sent by the k-th UE, where $i_k \in \{1, ..., \tau_p\}$ denotes the index of the pilot used by the k-th UE. We note by $\mathbf{\Theta} = \left[\theta_1, ..., \theta_{\tau_p}\right] \in \mathbb{C}^{\tau_p \times \tau_p}$ the pilot book matrix. Then, the UE k sends $\sqrt{\eta_k^u}\theta_{i_k}^H$, where η_k^u is the UL normalized transmit power. Let $\mathcal{P}_k \subset \{1, ..., K\}$ be the subset of UEs that use the same pilot as the k-th UE, including itself. As you can see, i_k and $\mathcal{P}_k$ do not depend on the RB index so that the pilot assignment is identical for all RBs, thanks to the orthogonality ensured by OFDM. Note that the pilot sequences are normalized such that $\theta_{i_k}^H \theta_{i_k} = \tau_p$ and 0 otherwise. The frequency-domain pilot signal received at the l-th AP on the $n\prime$-th RB is given by

$$\mathbf{Y}_{n\prime,l} = \sum_{k=1}^{K} \mathbf{h}_{n\prime,l,k} \sqrt{\eta_k^u} \theta_{i_k}^H + \mathbf{B}_l \in \mathbb{C}^{M \times \tau_p}, \tag{2}$$

where $\mathbf{B}_l \in \mathbb{C}^{M\times\tau_p}$ is a Gaussian noise matrix whose elements are i.i.d. $\mathcal{CN}(0,1)$.

In order to be compliant with the recent literature, we adopt, in this work, the *minimum mean square error* (MMSE) channel estimation method and the *pilot-to-precoder mapping* strategy inspired from the work in [11]. Hence, the frequency-domain channel estimate between the l-th AP and the k-th UE, corresponding to the $n\prime$-th RB can be given by

$$\hat{\mathbf{h}}_{n\prime,l,k} = c_{l,k}\bar{\mathbf{H}}_{n\prime,l}\mathbf{e}_{\mathbf{i_k}}, \tag{3}$$

where

- $c_{l,k}$ is a frequency independent scalar, which is defined as [31]

$$c_{l,k} \triangleq \frac{\sqrt{\eta_k^u}\beta_{l,k}}{\tau_p \sum_{t\in\mathcal{P}_k}\eta_t^u\beta_{l,t}+1} \tag{4}$$

- $\bar{\mathbf{H}}_{n\prime,l} \in \mathbb{C}^{M\times\tau_p}$ denotes the corresponding full-rank matrix of the frequency-domain channel estimates and is computed as

$$\bar{\mathbf{H}}_{n\prime,l} = \mathbf{Y}_{n\prime,l}\mathbf{\Theta} \tag{5}$$

- $\mathbf{e}_{\mathbf{i_k}}$ is the i_k-th column of $\mathbf{I}_{\tau_p}$, i.e., taking the i_k-th column of $c_{l,k}\bar{\mathbf{H}}_{n\prime,l}$.

Note that the channel estimates and estimation error, corresponding to the $n\prime$-th RB, which are denoted by $\hat{\mathbf{h}}_{n\prime,l,k}$ and $\tilde{\mathbf{h}}_{n\prime,l,k} = \mathbf{h}_{n,l,k} - \hat{\mathbf{h}}_{n\prime,l,k}$, are independent and distributed as $\hat{\mathbf{h}}_{n\prime,l,k} \sim \mathcal{CN}(\mathbf{0}, \gamma_{l,k}\mathbf{I}_M)$, $\tilde{\mathbf{h}}_{n\prime,l,k} \sim \mathcal{CN}(\mathbf{0}, (\beta_{l,k}-\gamma_{l,k})\mathbf{I}_M)$, where

$$\gamma_{l,k} \triangleq \frac{\eta_k^u\tau_p\beta_{l,k}^2}{\tau_p \sum_{t\in\mathcal{P}_k}\eta_t^u\beta_{l,t}+1} \tag{6}$$

Note that $\gamma_{l,k}$, which is the mean-square of the channel estimate between the AP l and the UE k, is antenna and frequency independent.

Remark 1 *(Per-RB to per-subcarrier channel mapping)* The channels at AP l are estimated per-RB and are assumed to be identical for RUs within one RB. Then, each AP can effectively construct τ_p channel coefficients per-subcarrier n as

$$\hat{\mathbf{h}}_{n,l,k} = \hat{\mathbf{h}}_{n\prime,l,k} \text{ for } n \in \text{RB}_{n\prime}, \tag{7}$$

we can also write

$$\bar{\mathbf{H}}_{n,l} = \bar{\mathbf{H}}_{n\prime,l} \text{ for } n \in \text{RB}_{n\prime}. \tag{8}$$

2) Basic OFDM based Downlink Data Transmission: The information data to be transmitted to the K users on the n-th subcarrier, which is denoted by $\mathbf{s}_n \in \mathbb{C}^{K\times 1}$, has independent elements with unit power, i.e., $E\left\{\|\mathbf{s}_n\|^2\right\} = 1$. Typically, OFDM systems specify certain unused subcarriers, as guard-band located at both ends of the spectrum. Hence, we divide the set of available subcarriers into two subsets: *(i)* Ξ, used for data transmission and *(ii)* its complementary Ξ^c, used for guard-band. Then, $\mathbf{s}_n = \mathbf{0}_{K\times 1}$ for $n \in \Xi^c$, i.e., no data is transmitted on the guard-band.

Precoding is needed to be performed at each AP in order to remove the multi-user interference (MUI) at receivers. In CF-mMIMO, the local nature of the implemented precoders is crucial to preserve system scalability. To stress this aspect, we use the terminology *local* precoding.

The signal vectors $\mathbf{s}_n, \forall n$, can be linearly precoded, at the l-th AP, as

$$\mathbf{x}_{l,n} = \mathbf{W}_{l,n}\mathbf{P}_l\mathbf{s}_n, \tag{9}$$

where:

- $\mathbf{x}_{l,n} \in \mathbb{C}^{M\times 1}$ denotes the precoded vector that contains samples to be transmitted over the the n-th subcarrier through the M antennas of AP l,
- $\mathbf{W}_{l,n} \in \mathbb{C}^{M\times K}$ is the precoding matrix corresponding to the n-th subcarrier at the l-th AP,
- $\mathbf{P}_l \in \mathbb{C}^{K\times K}$, which is frequency independent, represents a diagonal matrix whose elements $\sqrt{\eta_{l,k}}, k = 1, ..., K$ are the normalized transmit powers allocated to the K UEs.

To be compliant with the 5G standard, we consider max-min fairness power control that consists in maximizing the lowest user's downlink SE. Then, the *normalized* transmit power (normalized by the noise power σ_b^2) at each AP l, denoted by $\|\mathbf{x}_{l,n}\|^2 = \sum_{k=1}^{K} \eta_{l,k}, \forall n$ has to be constrained as $\sum_{k=1}^{K} \eta_{l,k} \leq \eta_l^{max}$, where

$$\eta_l^{max} = \frac{1}{\sigma_b^2}\frac{M(V_{sat}/G)^2}{\text{IBO}}, \tag{10}$$

where the IBO denotes the input back-off which represents the PA input power level relative to input saturation power, V_{sat} is PA amplitude saturation level and G is the PA linear gain.

The power control optimization problem can be formulated as follows [11][25]

$$\underset{\{\eta_{l,k}\geq 0\}}{maximize}\ \min_{k}\ \text{SINR}_{k,n} \tag{11}$$

$$s.t.\ \sum_{k=1}^{K}\eta_{l,k} \leq \eta_l^{max},\ \forall l \tag{12}$$

where $\text{SINR}_{k,n}$ denotes the signal-to-interference plus noise ratio (SINR) for user k at subcarrier n.

For the sake of self-containment, we consider, in this paper, the distributed power control policy where the power control coefficients are given in [11] as

$$\eta_{l,k} = \frac{\gamma_{l,k}}{\sum_{i=1}^{K}\gamma_{l,i}}\eta_l^{max},\ \forall l, \forall k \tag{13}$$

Inspired by [4][11][25] that study *local* precoding schemes in the downlink, we will consider the following linear precoders in frequency-domain of our OFDM based CF-mMIMO: (i) *local* full-pilot zero-forcing (FZF) and (ii) *local* regularized zero-forcing (RZF) . Here, the precoding vector employed by the l-th AP towards the k-th UE on subcarrier n, denoted by $\mathbf{w}_{l,n,i_k} \in \mathbb{C}^{M\times 1}$, is

$$\mathbf{w}_{l,n,i_k} = \begin{cases} \frac{\bar{\mathbf{H}}_{l,n}\left(\bar{\mathbf{H}}_{l,n}^H\bar{\mathbf{H}}_{l,n}\right)^{-1}\mathbf{e}_{i_k}}{\sqrt{E\left\{\|\bar{\mathbf{H}}_{l,n}\left(\bar{\mathbf{H}}_{l,n}^H\bar{\mathbf{H}}_{l,n}\right)^{-1}\mathbf{e}_{i_k}\|^2\right\}}} = \sqrt{(M-\tau_p)\theta_{l,k}}\bar{\mathbf{H}}_{l,n}\left(\bar{\mathbf{H}}_{l,n}^H\bar{\mathbf{H}}_{l,n}\right)^{-1}\mathbf{e}_{i_k}, & \text{for } \textit{local} \text{ FZF} \\ \frac{\hat{\mathbf{H}}_{l,n}\left(\hat{\mathbf{H}}_{l,n}^H\hat{\mathbf{H}}_{l,n}\right)^{-1}\hat{\mathbf{e}}_k}{\sqrt{E\left\{\|\hat{\mathbf{H}}_{l,n}\left(\hat{\mathbf{H}}_{l,n}^H\hat{\mathbf{H}}_{l,n}+\mathbf{P}_l^{-1}\right)^{-1}\hat{\mathbf{e}}_k\|^2\right\}}}, & \text{for } \textit{local} \text{ RZF} \end{cases} \tag{14}$$

where:

- $\theta_{l,k}$, which is the mean square of $\bar{\mathbf{H}}_{l,n}\mathbf{e}_{i_k}$, can be defined as $\theta_{l,k} = \gamma_{l,k}/c_{l,k}^2$ [11],

- $\hat{\mathbf{H}}_{l,n} \in \mathbb{C}^{M\times K}$ is the matrix of the channel estimates between the AP l and the K users on the subcarrier n, which can be collected as $\hat{\mathbf{H}}_{l,n} = \left[\hat{\mathbf{h}}_{l,n,1}, ..., \hat{\mathbf{h}}_{l,n,K}\right]$,
- $\mathbf{P}_l \in \mathbb{R}^{K\times K}$ is a diagonal regularization matrix,
- $\mathbf{e}_{i_k}$ is the k-th column of $\mathbf{I}_K$, i.e., taking the k-th column of $\hat{\mathbf{H}}_{l,n}\left(\hat{\mathbf{H}}_{l,n}^H\hat{\mathbf{H}}_{l,n}\right)^{-1}$.

Remark 2: It is worth mentioning that any AP can design the different aforementioned precoders by only using its local CSI. Exceptionally for the *local* FZF, it works only when $M \geq \tau_p + 1$ as explained in [11] and [25].

In order to perform the OFDM modulation at each antenna of an AP l, one need to reorder the M-dimensional precoded vectors $\{\mathbf{x}_{l,n}, \forall n\}$ to M transmit antennas (see Fig. 1) according to the following one-to-one mapping

$$\left[\mathbf{x}_{l,1}^t, ..., \mathbf{x}_{l,M}^t\right]^T = \left[\mathbf{x}_{l,1}, ..., \mathbf{x}_{l,N}\right], \tag{15}$$

where $\mathbf{x}_{l,m}^t \in \mathbb{C}^{1\times N}$ denotes the frequency-domain vector to be transmitted through the m-th antenna. Then, the OFDM modulated (time-domain) signals, performed at AP l, $\{\breve{\mathbf{a}}_{l,m}^t, \forall m\}$, are obtained by applying an inverse fast Fourier transform (IFFT) to $\{\mathbf{x}_{l,m}^t, \forall m\}$. Then, a cyclic prefix (CP) is added, at each antenna, to the time-domain samples, avoiding inter-symbol interference (ISI) to be occurred. It is clear that when the CP is larger than the channel length (T), the input-output relation of wireless channel can be specified in frequency-domain only.

One of the major drawbacks of OFDM is related to the fact that its time-domain signal has very high amplitude fluctuations, making it power-hungry as well as very sensitive to hardware impairments. These fluctuations are characterised by the peak-to-average power ratio (PAPR), which is defined as the ratio of the highest signal peak power and its average power value. Then, the PAPR, corresponding to the signal at antenna m of AP l, can be given by

$$PAPR(\breve{\mathbf{a}}_{l,m}^t) = \frac{\underset{0\leq t\leq LN-1}{max}\left[|\breve{a}_{l,m}(t)|^2\right]}{E\left\{|\breve{a}_{l,m}(t)|^2\right\}}, \tag{16}$$

where $\breve{\mathbf{a}}_{l,m}^t = [\breve{a}_{l,m}(0), ..., \breve{a}_{l,m}(LN-1)]$ and L denotes the oversampling factor.

3) Power amplifier model: In the case of NL OFDM based CF-mMIMO, the modulated signals $\{\mathbf{a}_{l,m}^t, \forall m\}$ are fed, towards each AP antennas, through M transmit chains with power amplifiers (PAs). The resulting amplified signal at antenna m of AP l cab be written as

$$\breve{\mathbf{z}}_{l,m}^t = \mathbf{f}\left(\breve{\mathbf{a}}_{l,m}^t\right) \tag{17}$$

where $\mathbf{f}(.)$ represents the nonlinear amplification operation which is assumed to be identical over all antennas of all APs, for the sake of simplicity. Specifically, the nonlinear behavior of the PA can be modeled by the following full-rank polynomial

$$\breve{z}_{l,m}(n) = \sum_{i=1}^{I} \lambda_i \breve{a}_{l,m}(n)|\breve{a}_{l,m}(n)|^{i-1}, \tag{18}$$

where $\lambda_1, ..., \lambda_I$ are complex-valued model parameters that capture both amplitude-to-amplitude (AM/AM) and amplitude-to-phase (AM/PM) conversions. We have neglected the memory effects because we are primarily looking for how the basic nonlinear distortions are processed and tackled within highly-efficient OFDM based CF-mMIMO.

According to the Busgang theorem [32], the time-domain OFDM signal at the output of the NL PA can be expressed as

$$\breve{\mathbf{z}}_{l,m}^{t} = K_0 \breve{\mathbf{a}}_{l,m}^{t} + \breve{\mathbf{d}}_{l,m}^{t} \tag{19}$$

where K_0 is a complex gain which is frequency independent and $\breve{\mathbf{d}}_{l,m}^{t}$ is a zero mean noise which is uncorrelated with $\breve{\mathbf{a}}_{l,m}^{t}$. This latter is not Gaussian, but at the receiver side, after the OFDM demodulation, it becomes Gaussian.

Note that these nonlinear distortion (NLD) parameters can be computed analytically, letting us to be able to develop closed-form expression to evaluate the in-band performance of CF-mMIMO-OFDM systems. For the sake of self-containment, we herein present, in equations (20) and (21), the closed-form expressions for the NLD parameters in terms of the model PA parameters $\{\lambda_i\}$. Such expressions were already given in [33] and [34].

$$\begin{aligned} K_0 = \lambda_1 &+ \sqrt{\frac{\pi}{8}} \sum_{i=2,\ i\ even}^{I} (i+1)\lambda_i \sigma^{i-1} \prod_{i\prime=0}^{\frac{i-2}{2}} (2i\prime+1) \\ &+ \frac{1}{2} \sum_{i=3,\ i\ odd}^{I} (i+1)\lambda_i (\sqrt{2}\sigma)^{i-1} (\frac{i-1}{2})! \end{aligned} \tag{20}$$

and

$$\begin{aligned} \sigma_d^2 = &\sum_{i=1}^{I} |\lambda_i|^2 \, 2^i \sigma^{2i} i! - 2\,|K_0|^2 \sigma^2 \\ &+ \sqrt{\frac{4\pi}{2}} \sum_{i,l=1, i\neq l,\ (i+l)\ odd}^{I} \Re[\lambda_i \lambda_l^*] \sigma^{i+l} \prod_{i\prime=0}^{\frac{i+l-1}{2}} (2i\prime+1) \\ &+ 2 \sum_{i,l=1, i\neq l,\ (i+l)\ even}^{I} \Re[\lambda_i \lambda_l^*] (\sqrt{2}\sigma)^{i+l} (\frac{i+l}{2})! \end{aligned} \tag{21}$$

where σ is the standard deviation of the PA input signal.

The frequency-domain received signal at UE k and subcarrier n can be given by

$$\begin{aligned} y_{k,n} &= \sum_{l=1}^{L} \mathbf{h}_{l,k,n}^{H} \mathbf{z}_{l,n} + b_{k,n} \\ &= \sum_{l=1}^{L} \mathbf{h}_{l,k,n}^{H} \left(\mathbf{K}_0 \mathbf{x}_{l,n} + \mathbf{d}_{l,n}\right) + b_{k,n} \\ &= \sum_{l=1}^{L} \mathbf{h}_{l,k,n}^{H} \mathbf{K}_0 \mathbf{x}_{l,n} + \sum_{l=1}^{L} \mathbf{h}_{l,k,n}^{H} \mathbf{d}_{l,n} + b_{k,n} \end{aligned} \tag{22}$$

where $\mathbf{z}_{l,n} \in \mathbb{C}^{M\times 1}$ denotes the frequency-domain amplified signal transmitted by AP l on subcarrier n, $\mathbf{d}_{l,n} \in \mathbb{C}^{M\times 1}$ is the frequency-domain version of NLD noise, $\mathbf{K}_0$ is the $M \times M$ diagonal matrix whose elements are equal to K_0 and $b_{k,n} \sim \mathcal{CN}(0,1)$ is an i.i.d. Gaussian noise.

III. Performance Analysis

By plugging (9) in (22), $y_{k,n}$ can be expanded as

$$y_{k,n} = \sum_{l=1}^{L} \mathbf{h}_{l,k,n}^H \mathbf{K}_0 \mathbf{W}_{l,n} \mathbf{P}_l \mathbf{s}_n + \sum_{l=1}^{L} \mathbf{h}_{l,k,n}^H \mathbf{d}_{l,n} + b_{k,n} \tag{23}$$
$$= \underbrace{\sum_{l=1}^{L} \sqrt{\eta_{l,k}} \mathbf{h}_{l,k,n}^H \mathbf{K}_0 \mathbf{w}_{l,n,i_k} s_{k,n}}_{\text{Desired signal}} + \underbrace{\sum_{l=1}^{L} \sum_{t \neq k}^{K} \sqrt{\eta_{l,t}} \mathbf{h}_{l,k,n}^H \mathbf{K}_0 \mathbf{w}_{l,n,i_t} s_{t,n}}_{\text{Multi-user interference}} + \underbrace{\sum_{l=1}^{L} \mathbf{h}_{l,k,n}^H \mathbf{d}_{l,n}}_{\text{PA impairments}} + \underbrace{b_{k,n}}_{\text{Noise}}$$

One can note that $y_{k,n}$ consists of four terms: (i) the desired signal for the UE k, (ii) the multi-user interference, (iii) the NLD noise caused by the different PAs in the L APs and (iv) the noise.

It is the third term (PA impairments) together with the adoption of OFDM and several *local* precoders that makes the analysis in this paper different from existing literature. In the following, we will use (23) to derive the downlink SE and EE.

A. Downlink Spectral Efficiency

Inspired by works [4][11][25][35] that apply a bounding technique, referred to as hardening bound, we derive the achievable downlink SE, i.e., a lower bound on the ergodic capacity, for OFDM based CF-mMIMO under PA non-linearity and the assumption of independent Rayleigh fading channel. Towards this end, we rewrite (23), in frequency-domain, as

$$y_{k,n} = \underbrace{\text{CP}_{k,n}}_{\text{Coherent precoding}} s_{k,n} + \underbrace{\text{PGU}_{k,n}}_{\text{Precoding gain uncertainly}} s_{k,n} + \sum_{t \neq k}^{K} \underbrace{\text{MUI}_{kt,n}}_{\text{Multi-user interference}} s_{t,n} + \underbrace{\text{PAI}_{k,n}}_{\text{PA impairments}} + \underbrace{b_{k,n}}_{\text{Noise}} \tag{24}$$

where the coherent precoding $\text{CP}_{k,n}$ is given by

$$\text{CP}_{k,n} = \sum_{l=1}^{L} \sqrt{\eta_{l,k}} \text{E}\left\{ \mathbf{h}_{l,k,n}^H \mathbf{K}_0 \mathbf{w}_{l,n,i_k} \right\}, \tag{25}$$

the precoding gain uncertainly $\text{PGU}_{k,n}$ can be written as

$$\text{PGU}_{k,n} = \sum_{l=1}^{L} \sqrt{\eta_{l,k}} \left(\mathbf{h}_{l,k,n}^H \mathbf{K}_0 \mathbf{w}_{l,n,i_k} - \text{E}\left\{ \mathbf{h}_{l,k,n}^H \mathbf{K}_0 \mathbf{w}_{l,n,i_k} \right\} \right), \tag{26}$$

the multi-user interference $\text{MUI}_{kt,n}$ can be expressed as

$$\text{MUI}_{kt,n} = \sum_{l=1}^{L} \sqrt{\eta_{l,t}} \mathbf{h}_{l,k,n}^H \mathbf{K}_0 \mathbf{w}_{l,n,i_t}, \tag{27}$$

and the PA impairments $\text{PAI}_{k,n}$ is given by

$$\text{PAI}_{k,n} = \sum_{l=1}^{L} \mathbf{h}_{l,k,n}^H \mathbf{d}_{l,n} \tag{28}$$

We recall that $\mathbf{d}_{l,n}$ is uncorrelated with $s_{k,n}$, i.e., the first term is uncorrelated with the fourth term. Moreover, it is clear that the first term is also uncorrelated with the second and third terms since, respectively, $s_{k,n}$ is independent of $\text{PGU}_{k,n}$ and $s_{k,n}$ and $s_{t,n}$ are uncorrelated $\forall\ t \neq k$. Therefore, the sum of the second, third, fourth and fifth terms in (24) can be seen as an uncorrelated effective noise, when assuming that the fifth term (noise) is assumed to be independent of the first term. Hence, the SINR can be given as stated in **Corollary 1**.

***Corollary 1**:* The effective SINR of UE k at subcarrier n is given by

$$\begin{aligned}\mathrm{SINR}_{k,n} &= \frac{|\mathrm{CP}_{k,n}|^2}{\mathrm{E}\left\{|\mathrm{PGU}_{k,n}|^2\right\} + \sum_{t\neq k}^{K}\mathrm{E}\left\{|\mathrm{MUI}_{kt,n}|^2\right\} + \mathrm{E}\left\{|\mathrm{PAI}_{k,n}|^2\right\} + 1} \\ &= \frac{\left|\sum_{l=1}^{L}\sqrt{\eta_{l,k}}\mathrm{E}\left\{\mathbf{h}_{l,k,n}^{H}\mathbf{K}_0\mathbf{w}_{l,n,i_k}\right\}\right|^2}{\sum_{t=1}^{K}\mathrm{E}\left\{\left|\sum_{l=1}^{L}\sqrt{\eta_{l,t}}\mathbf{h}_{l,k,n}^{H}\mathbf{K}_0\mathbf{w}_{l,n,i_t}\right|^2\right\} - \left|\sum_{l=1}^{L}\sqrt{\eta_{l,k}}\mathrm{E}\left\{\mathbf{h}_{l,k,n}^{H}\mathbf{K}_0\mathbf{w}_{l,n,i_k}\right\}\right|^2 + \mathrm{E}\left\{\left|\sum_{l=1}^{L}\mathbf{h}_{l,k,n}^{H}\mathbf{d}_{l,n}\right|^2\right\} + 1}\end{aligned} \tag{29}$$

Then, the per-RB SE of a user k is lower bounded as stated by **Corollary 2**.

***Corollary 2**:* The per-RB and per-user SE in the downlink is given by

$$\mathrm{SE}_k = \xi\left(1 - \frac{\tau_p}{N_{sc}N_c}\right)N_{sc}\Delta f \log_2\left(1 + \mathrm{SINR}_{k,n}\right), \tag{30}$$

where Δf denotes the subcarrier spacing.

Note that this SE expression is valid for all precoding schemes presented in (14) and analytical expressions regarding the FZF scheme are stated by **Corollary 3**. Note that closed-form expression for the *local* RZF is intractable and only results, performed by Monte-Carlo simulations, are presented regarding this latter precoding scheme.

Corollary 3**:* The per-user downlink SE (bit/s) is obtained for FZF precoding as in ***Corollary 2, where

$$\mathrm{SINR}_{k,n} = \frac{(M-\tau_p)|K_0|^2\left(\sum_{l=1}^{L}\sqrt{\eta_{l,k}\gamma_{l,k}}\right)^2}{(M-\tau_p)|K_0|^2\sum_{t\in\mathcal{P}_k\setminus\{k\}}\left(\sum_{l=1}^{L}\sqrt{\eta_{l,t}\gamma_{l,k}}\right)^2 + |K_0|^2\sum_{l=1}^{L}\sum_{t=1}^{K}\eta_{l,t}(\beta_{l,k}-\gamma_{l,k}) + \Psi_{k,n} + 1}, \tag{31}$$

where $\Psi_{k,n}$ denotes the NLD variance which can be expressed as

$$\begin{aligned}\Psi_{k,n} &= \mathrm{E}\left\{\left|\sum_{l=1}^{L}\mathbf{h}_{l,k,n}^{H}\mathbf{d}_{l,n}\right|^2\right\} \\ &= \sum_{l=1}^{L}\sum_{l\prime=1}^{L}\sum_{m=1}^{M}\sum_{m\prime=1}^{M}\mathrm{E}\left\{h_{l,k,n,m}^{*}d_{l,n,m}d_{l\prime,n,m\prime}^{*}h_{l\prime,k,n,m\prime}\right\}\end{aligned} \tag{32}$$

***Proof**:* see Appendix.

Note that $\Psi_{k,n}$ depends on both intra-user and inter-user nonlinear distortion, which can not be eliminated by using conventional transmit precoding techniques. Moreover, the behavior of this NLD depends on many parameters, such as number of users, number of pilots, number of APs, number antennas per-AP, the precoding scheme, channel estimation, pilot contamination and essentially the adopted PA and its operating point.

In order to derive closed-from expressions for the SINR of the k-th user at the n-th subcarrier, it is remaining to find the terms in (32). Note that due to the possibility of NLD correlation, these latter are not necessary zero even when $l \neq l\prime$ and $m \neq m\prime$. But, it is still possible to have closed-form expressions, for $\Psi_{k,n}$, corresponding to some scenarios as stated in ***Lemma 1***, corresponding to FZF precoding.

***Lemma 1** (NL OFDM based CF-mMIMO with local FZF precoding):* With FZF precoding, when $\tau_p \to M$, Ψ_k can be expressed as

$$\Psi_k^{FZF} = \frac{M}{\sigma_b^2}\sum_{l=1}^{L}\beta_{l,k}\sigma_d^2, \tag{33}$$

and achievable SE for the k-th UE can be defined as stated in ***Theorem 1***.

Theorem 1*:* In OFDM based CF-mMIMO adopting nonlinear PA and FZF precoding ($\tau_p \rightarrow M$), the downlink capacity of the k-th UE is lower bounded by

$$\mathrm{SE}_k = \chi N_{sc} \Delta f \log_2 \left(1 + \frac{(M-\tau_p)|K_0|^2 \left(\sum_{l=1}^{L} \sqrt{\eta_{l,k}\gamma_{l,k}} \right)^2}{(M-\tau_p)|K_0|^2 \sum_{t \in \mathcal{P}_k \setminus \{k\}} \left(\sum_{l=1}^{L} \sqrt{\eta_{l,t}\gamma_{l,k}} \right)^2 + |K_0|^2 \sum_{l=1}^{L} \sum_{t=1}^{K} \eta_{l,t}(\beta_{l,k} - \gamma_{l,k}) + \Psi_k^{FZF} + 1} \right), \tag{34}$$

where χ, which denotes the percentage of DL payload data, is expressed as $\chi = \xi \left(1 - \frac{\tau_p}{N_{sc} N_c}\right)$ and we recall that σ_d^2 is given in closed-form in (21).

Proof*:* see Appendix.

B. Downlink Energy Efficiency

In this subsection, we derive the EE of OFDM based CF-mMIMO systems to investigate how it is affected by the PA's IBO and the number of APs. Inspired by [36][37][38], we consider the per-RB EE as the ratio of the sum rate (bits/s) to the total system power consumption (Watt). The per-RB EE is defined as

$$\mathrm{EE} = \frac{\sum_{k=1}^{K} \mathrm{SE}_k}{P_{total}}, \tag{35}$$

where P_{total} can be defined as [36]

$$P_{total} = \sum_{l=1}^{L} P_l + \sum_{l=1}^{L} P_{fh,l}, \tag{36}$$

where P_l denote the power consumption at the l-th AP due to the RF and digital processing, i.e., the PA and the circuit power consumption, and $P_{fh,l}$ is the power consumed by the front-haul link connecting the l-th AP with the CPU.

The P_l can be modeled as

$$P_l = \sigma_b^2 \frac{M}{\mu_l} \left(\sum_{k=1}^{K} \eta_{l,k} \gamma_{l,k} \right) + M P_{c,l}, \tag{37}$$

where $0 < \mu_l \leq 1$ is the power amplifier efficiency, which can be expressed in terms of IBO as $\mu_l = \mu_{max}/\sqrt{IBO}$, where μ_{max} is the maximum power efficiency; and $P_{c,l}$ is the consumed power related to each antenna to run the circuit components.

In Downlink CF-mMIMO, the front-hauling cost refers to the amount of data to be transferred between the CPU and the APs to satisfy coherent transmission and other centralized network operations. Since all processing related to the precoding and PAPR reduction are fully distributed (i.e. they do not need any exchange of information), the CPU need to send, within a coherence block, $|\Xi|\tau_D KL$ complex samples (i.e., $\{s_{k,n}\}$). Inspired by [36], the front-haul power consumption is proportional to the sum spectral efficiency, as follows

$$P_{fh,l} = P_{0,l} + P_{bt,l} \sum_{k=1}^{K} \mathrm{SE}_k, \tag{38}$$

where $P_{0,l}$ is a fixed power consumption which depends on link between the AP l and the CPU, and $P_{bt,l}$ is the traffic-dependent power.

For the sake of clarity and without loss of generality, we assume that all APs have the same transceiver model (i.e., $\mu_l = \mu \ \forall l$ and $P_{c,l} = P_c \ \forall l$); and $P_{0,l}$ and $P_{bt,l}$ are AP-independent, such that $P_{0,l} = P_0 \ \forall l$ and $P_{bt,l} = P_{bt} \ \forall l$. To this end, the per-RB EE can be written as

$$\text{EE} = \frac{\sum_{k=1}^{K} \text{SE}_k}{\frac{M\sigma_b^2}{\mu} \sum_{l=1}^{L} \sum_{k=1}^{K} \eta_{l,k}\gamma_{l,k} + LMP_c + LP_0 + LP_{bt} \sum_{k=1}^{K} \text{SE}_k}, \tag{39}$$

IV. Proposed local PAPR reduction algorithm

A. Discussion

In classical (co-located) massive MIMO systems, a high-dimensional degrees of freedom (DoFs) are offered by equipping the BS with a large number of antennas compared to the number of served users. Interestingly, these DoFs can be exploited to effectively reduce the PAPR of transmit signals [20][21][22][23][24]. In centralized CF-mMIMO, i.e., adopting high capacity front-haul connections to transfer data between the APs and the CPU, it would be possible to re-use the PAPR reduction methods already proposed for co-localised mMIMO. However, the PAPR reduction and its associated energy-efficiency improvement will be in the cost of heavy front-hauling load, leading to reduced global system energy-efficiency.

In this regard, we propose new PAPR reduction technique that is performed locally at each AP, with no instantaneous information sharing (e.g. CSI), leading to a reduced front-hauling overhead. Consequently, it becomes very challenging to find a solution that is able to provide considerable PAPR reduction while it is constrained to i) be implementable with APs adopting few antennas ii) do not need additional front-hauling overhead and iii) do not damaging the transmission quality.

The principle behind our proposed solution (see Fig. 1) is that each AP 1) computes the frequency-domain precoded signals $\{\mathbf{x}_m^t, \forall m\}$, which are the reordered versions of $\{\mathbf{x}_n, \forall n\}$ and 2) optimize frequency-domain signals $\{\mathbf{r}_m^t, \forall m\}$, referred to as peak-canceling signals (PCSs), that reduce the PAPR of the resulting OFDM modulated signals $\{\breve{\mathbf{a}}_m^t, \forall m\}$. It is worth mentioning that, for the sake of simplicity, the index l is removed.

Therefore, $\{\mathbf{r}_m^t, \forall m\}$ are designed such that their time-domain versions, $\{\breve{\mathbf{r}}_m^t, \forall m\}$, minimize the maximum of $\{\breve{\mathbf{a}}_m^t, \forall m\}$ as

$$\begin{aligned} \{\mathbf{r}_1^{t,\text{opt}}, .., \mathbf{r}_M^{t,\text{opt}}\} &= \underset{\{\mathbf{r}_m^t\}}{\text{argmin}} \ \max \left\{ \|\breve{\mathbf{a}}_1^t\|_\infty, ..., \|\breve{\mathbf{a}}_M^t\|_\infty \right\} \\ &= \underset{\{\mathbf{r}_m^t\}}{\text{argmin}} \ \max \left\{ \|IDFT\left(\mathbf{x}_1^t + \mathbf{r}_1^t\right)\|_\infty, ..., \|IDFT\left(\mathbf{x}_M^t + \mathbf{r}_M^t\right)\|_\infty \right\} \end{aligned} \tag{40}$$

The key idea of the proposed solution is to anticipate the distortion, so that instead of transmitting high-PAPR signals through NL PAs that cause severe distortions (not controllable at all), we transmit low-PAPR signals (avoiding such severe PA-related distortion) by generating the PCSs $\{\mathbf{r}_m^t, \forall m\}$ which can add distortion to the transmitted signals but, interestingly, we can control it. Indeed, PA-related distortion is proportional to the amount of the power allocated to the desired signal, making the *strongest* users, i.e. having the largest channel gains, to be the most affected and, without interest, the *weakest* users to be less affected.

Towards this end, we optimize the PCSs that satisfy the ***Statement 1***.

***Statement 1**:* Frequency-domain peak-cancelling signals are optimized such that distortion caused to the *strongest* users is negligible or even null while distortion caused to the *weakest* users are tolerable. **Specifically, the PCS-related distortions are constrained to be beam-formed only towards the *weakest* users in a flexible way, so that we continue to provide service for these latter.**

More specifically, each AP l divides the set of active users into two disjoint subsets: strong users, $\Omega_l \subset \{1, ..., K\}$, and weak users, $\Omega_l^c \subset \{1, ..., K\}$, where $\Omega_l \cap \Omega_l^c = \emptyset$ and $|\Omega_l| + |\Omega_l^c| = K$.

The user grouping is based on the user path-loss: the τ_s users having the highest path-losses belong to Ω_l, while $\tau_p - \tau_s$ users belong to Ω_l^c. Note that if UE $k \in \Omega_l$, any UE $t \in \mathcal{P}_k$ belongs to Ω_l.

B. Computing frequency-domain peak-canceling signals (PCSs)

We discuss, in this subsection, how to design the optimal frequency-domain PCSs $\{\mathbf{r}_n, \forall n\}$, at each AP l, to perform the best PAPR reduction performance while keeping good transmission quality. It consists in fitting, iteratively, these PCSs to time-domain clipping-noise signals, denoted by $\{\mathbf{e}_n, \forall n\}$, that give the desired PAPR. These latter are computed by clipping the time-domain signals $\{\mathbf{a}_m^t, \forall m\}$, at each antenna. The clipped signals can be obtained as follows

$$\bar{\breve{a}}_m(t) \quad = \begin{cases} \breve{a}_m(t), & \textit{if } |\breve{a}_m(t)| < \delta \\ \delta e^{j\phi(t)}, & \textit{if } |\breve{a}_m(t)| > \delta \end{cases}, \tag{41}$$

where $\breve{a}_m(t) = |\breve{a}_m(t)|e^{j\phi(t)}$, $\phi(t)$ is the phase of $\breve{a}_m(t)$ and δ denotes the clipping threshold.

In order to obtain the best PAPR reduction, δ should be related to the OFDM signal mean power and the percentage of the reserved users τ_p/τ_s. Then, it is chosen to be

$$\delta = \sqrt{\sigma^2 \left(\frac{\tau_p}{\tau_s}\right)}, \tag{42}$$

where σ^2 denotes the variance of the modulated signal at each antenna. It is worth to mention that δ has to satisfy the out-of-band constraint and should be $\delta \geq \sqrt{\sigma^2 ln\left(\frac{N}{N_a}\right)}$ [23], where $N_a = |\Xi|$ denotes the number of activated subcarriers.

Then, the original frequency-domain clipping-noise signal associated to the m-th transmit antenna is

$$\epsilon_m^t = DFT\left(\bar{\breve{\mathbf{a}}}_m - \breve{\mathbf{a}}_m\right). \tag{43}$$

Here, the vectors $\{\epsilon_n, \forall n\}$ are collected from the M vectors $\{\epsilon_1^t, \epsilon_2^t, ..., \epsilon_M^t\}$.

Plugging (43) into (40), we have

$$\{\mathbf{r}_1^{t,\text{opt}}, .., \mathbf{r}_M^{t,\text{opt}}\} = \underset{\{\mathbf{r}_m^t\}}{\text{argmin}} \max \left\{\|IDFT\left(\mathbf{x}_1^t + \left(\mathbf{r}_1^t - \epsilon_1^t\right)\right)\|_\infty, ..., \|IDFT\left(\mathbf{x}_M^t + \left(\mathbf{r}_M^t - \epsilon_M^t\right)\right)\|_\infty\right\} \tag{44}$$

According to (44), it is clear that the best PAPR is obtained when the PCSs, $\{\mathbf{r}_m^t\}$, equal the original clipping-noise signals $\{\epsilon_m^t\}$. However, the PCSs hardly equal the original peak-cancelling signals because the have to satisfy the necessary constraints. Indeed, the frequency-domain PCSs are obtained through a projection of the original frequency-domain clipping-noise signals, $\{\epsilon_m^t\}$, such that they satisfy the ***Statement 1***. In addition, they have to

respect the out-of-band constraint such that they have to be set to zero on the guard-band. Then, frequency-domain PCSs can be defined as

$$\mathbf{r}_n = \nu_l \mathbf{V}_{l,n} \epsilon_n, \ \forall n \ \in \ \Xi \tag{45}$$
$$\mathbf{r}_n = \mathbf{0}_{M_t \times 1}, \ \forall n \ \in \ \Xi^c$$

where :

- $\{\mathbf{r}_n\}$ are collected from the M vectors $\{\mathbf{r}_1^t, \mathbf{r}_2^t, ..., \mathbf{r}_M^t\}$
- $\mathbf{V}_{l,n} \in \mathbb{C}^{M \times M}$ represents the projection space corresponding to AP l, i.e., projection matrix (please refer to Section IV-C) and ν_l is a regularization factor (discussed in Section IV-D).

To efficiently reduce the PAPR, we propose an iterative method that aims at fitting the PCSs to the original clipping-noise.

C. Design of flexible projection space $\mathbf{V}_{l,n}$

To significantly protect the strong users, i.e., UEs in Ω_l, against the distortion caused by adding PCSs, we force the distortion to take place in the orthogonal complement of $\{\mathbf{h}_{l,k,n} \ \forall l, \ \forall n$ and $\forall k \ \in \ \Omega_l\}$. To do that, let

$$\mathbf{V}_{l,n} = \mathbf{I}_M - \bar{\mathbf{H}}_{l,n} \left(\bar{\mathbf{H}}_{l,n}^H \bar{\mathbf{H}}_{l,n} + \mathbf{\Gamma}_l \right)^{-1} \bar{\mathbf{H}}_{l,n}^H \tag{46}$$

denote the projection matrix, corresponding to AP l and subcarrier n, where $\mathbf{\Gamma}_l \in \mathbb{R}^{\tau_p \times \tau_p}$ is a regularized diagonal matrix that enables flexibility in how we project the distortion related the to PAPR reduction (i.e., adding PCSs).

Indeed, by using this projection matrix, we have $\nu_l \hat{\mathbf{h}}_{l,n,k} \mathbf{V}_{l,n} \epsilon_{l,n} = 0$, only if $\mathbf{\Gamma}_l [k,k] = 0$, meaning that distortion caused to the corresponding user k almost vanishes (only a small contribution can survive when channel estimation errors are occurred). Thus, $\mathbf{\Gamma}_l [k,k] = 0 \ \forall k \ \in \ \Omega_l$.

Conversely, $\nu_l \hat{\mathbf{h}}_{l,n,k\prime} \mathbf{V}_{l,n} \epsilon_{l,n} \neq 0$ when $\mathbf{\Gamma}_l [k\prime, k\prime] \neq 0$, meaning that there is distortion caused to UEs $k\prime$. In order to make this distortion tolerable, it would be scaled inversely proportional to the power allocated to user $k\prime$. Then, we define $\mathbf{\Gamma}_l [k\prime, k\prime] = 1/\eta_{l,k\prime} \ \forall k\prime \ \in \ \Omega_l^c$. To summarize, our approach guarantees full distortion protection to UEs with high channel gains, except for channel estimation errors, while still providing service to UEs with bad channel gains. It offers a good balance between PAPR reduction and cancelling distortion (adjustable by properly choosing τ_s). That is clear now the philosophy of our approach - *Reduce the PAPR and protect* -.

D. Computing the optimal value of ν_l

Due to the reconstruction of the precoded PCSs from their projections onto the projection matrix and the available data subcarriers in Ξ, it is obvious that the considered PCSs, at each iteration, can be smaller than their associated clipping noises when the traditional clipping and control (CC) method is employed at each AP. Hence, a regularization factor is needed in order to generate the optimal PCSs, leading then to a fast convergence toward the optimal solution. Then, ν_l is optimized such that $\nu_l \mathbf{V}_{l,n} \epsilon_{l,n}$ is similar to $\epsilon_{l,n}$. It can be calculated using least-square approximation (LSA), as explained in [23] as

$$\nu_l = \mathrm{E}_n \left[\frac{\sum_m |\mathbf{V}_{l,n} \epsilon_{l,n}| |\epsilon_n|}{\sum_m |\mathbf{V}_{l,n} \epsilon_{l,n}|^2} \right]. \tag{47}$$

Using such regularization factor, the amplitudes of PCSs $\nu_l \mathbf{V}_{l,n}\epsilon_{l,n}$ generated by LSA, almost equal to those of the original clipping noise ϵ_n. Then, we transmit $\nu_l \mathbf{V}_{l,n}\epsilon_{l,n}$ instead of $\mathbf{V}_n\epsilon_n$. This operation reduces the number of iterations to achieve the optimal PAPR reduction.

E. Algorithm Summary

In this subsection, we present our developed algorithm applying the above-explained PAPR reduction approach. The PAPR reduction based CF-mMIMO-OFDM DL tranmission is achieved by alternately repeating the PAPR reduction process using the clip and control (CC) appraoch and restoring the restrictions on the clipping-noise components using the proposed flexible projection space.

The details of the proposed algorithm is summarized in Table **Algorithm**. One can clearly see that the proposed algorithm proceeds in only one-loop where it performs the OFDM modulated signals in Step 6, the clipping-noise in Step 7, the OOB constraint in Step 8 and the optimal value of ν_l in Step 9. The peak-cancelling signals $\{\mathbf{r}_{l,n}\}$ are performed in Step 10. Finally, the precoded signals $\{\mathbf{x}_{l,n}\}$ are updated in Step 11.

Note that any intermediate solution can be used, ensuring good in-band transmission quality and without causing any OOB radiation.

Algorithm: The proposed *local*PAPR*free* algorithm

Given:

- a set of N modulated complex signals $\{\mathbf{s}_{k,n}\}$
- the channel estimates $\{\bar{\mathbf{H}}_{l,n}\}$, for $n = 1, .., N$
- the UEs path-losses $\{\beta_{l,k}\}$

1: **Define**:

- the two groups of users (*stong* and *weak*),
- the corresponding regularization diagonal matrix $\mathbf{\Gamma_1}$ (subsection IV-C)

2: **Compute**:

- the projection matrices $\{\mathbf{V}_{l,n}\}$, as given by equation (45)
- the precoded data vectors $\{\mathbf{x}_{l,n}\}$, as given by equation (9)

3: **Set** the maximal iteration number N_{iter}

4: **Initialize**:

- $\{\mathbf{r}_{l,n}^{(1)} = \mathbf{0}_{M\times 1}\}$
- $\{\mathbf{x}_{l,n}^{(1)}\} = \{\mathbf{x}_{l,n}\}$

5: **for** p=1,...,N_{iter} **do**

6: $\breve{\mathbf{a}}_m^{t(p)} = IFFT\left(\mathbf{x}_m^{t(p)}\right),\ \forall\ m = 1...M$

7: $\epsilon_m^{t(p)} = FFT\left(\bar{\mathbf{a}}_m^{t(p)} - \breve{\mathbf{a}}_m^{t(p)}\right)$

8: $\epsilon_{l,n}^{(p)} = \mathbf{0}_{M\times 1}$, for $n \in \chi^c$

9: $\nu_l = \mathrm{E}_n\left[\frac{\sum_m |\mathbf{V}_{l,n}\epsilon_{l,n}^{(p)}||\epsilon_n^{(p)}|}{\sum_m |\mathbf{V}_{l,n}\epsilon_{l,n}^{(p)}|^2}\right]$

10: $\mathbf{r}_{l,n}^{(p)} = \nu_l \mathbf{V}_{l,n}\epsilon_{l,n}^{(p)}$, for $n \in \chi$

11: $\mathbf{x}_n^{(p+1)} = \mathbf{x}_{l,n}^{(p)} + \mathbf{r}_{l,n}^{(p)},\ \forall n \in \chi$

12: **end for**

13: **return** $\{\mathbf{x}_{l,n}^{(Niter+1)}\}$

F. Complexity Analysis

As a complexity measure, we adopt the number of complex multiplications. For the developed *local*PAPR*free* algorithm, one can easily note that the added computational cost, compared with the original CF-mMIMO precoding scheme, is dominated by the N-points IFFT/FFT (Steps 6 and 7) and the projection operation in Step 10. The IFFT/FFT costs $\mathcal{O}(MN\log(N))$ and the projection costs $\mathcal{O}(M^2|\Xi|)$. Therefore, the *local*PAPR*free* requires a total of $\mathcal{O}(2MN\log(N)+M^2|\Xi|)$ complex multiplications for each iteration. Evidently, the number of iterations should be chosen judiciously to offer good balance between PAPR reduction and computational complexity. Note that since the computational complexity of the *local* FZF precoding scheme is about $MN\log(N)+N\left(\frac{3\tau_p^2 M}{2}+\frac{\tau_p M}{2}+\frac{\tau_p^3-\tau_p}{3}\right)$ [11], the added complexity related to our PAPR reduction algorithm is quite negligible.

V. Simulation Results

This section provides numerical results to evaluate the performance of OFDM based cell-free massive MIMO in terms of DL SE and DL EE, in presence of nonlinear power amplifiers. In addition, the benefit of our proposed PAPR reduction algorithm is evaluated.

A. Simulation Scenario

Let us introduce the considered CF-mMIMO-OFDM system setup. We assume that the L APs and the K UEs are independently and uniformly distributed within an area of size $D\times D$ squared meters, which is wrapped around at the edges to avoid boundary effects.

We consider an uncoded OFDM with IFFT/FFT of $N=256$ and use a spectral map Ξ, in which $N_a=|\Xi|=248$ are used for data transmission and $N_{gb}=|\Xi^c|=4$ are used as guard-band at each side. Thus $N=N_a+2N_{gb}=256$. The IFFT/FFT size is set to 1024, which corresponds to 4-oversampling in the time-domain to evaluate the PAPR accurately. Note that We consider an OFDM radio frame of duration 1 ms (corresponding to the channel coherence time), which consists of 14 OFDM symbols. From the frequency-domain perspective, each RB contains $N_{rb}=12$ subcarriers with 15 kHz of bandwidth each.

The large-scale fading coefficients $\{\beta_{l,k}\}$ are modeled as [11]

$$\beta_{l,k}=\text{PL}_{l,k}.10^{\frac{\sigma_{sh}z_{l,k}}{10}}, \tag{48}$$

where $\text{PL}_{l,k}$ denotes the path-loss and $10^{\frac{\sigma_{sh}z_{l,k}}{10}}$ models log-normal shadow fading with standard deviation σ_{sh} and $z_{l,k}\sim\mathcal{N}(0,1)$. Note that, in this investigation, we consider the 3GPP Urban Microcell path-loss model, which is given by equation (49) when assuming a 2 GHz carrier frequency [11][39].

$$\text{PL}_{l,k}\,[\text{dB}]=-30.5-36.7\log_{10}\left(\frac{d_{l,k}}{1\ m}\right), \tag{49}$$

where $d_{l,k}$ denotes the distance between the l-th AP and the k-th UE including AP and UE's heights.

The simulation settings are reported in Table I. Note that the PA characteristics are modeled by the memoryless modified Rapp model, defined by the 3GPP in [40], with parameters $G=16$, $V_{sat}=1.9$, $p=1.1$, $A=-345$, $B=0.17$ and $q=4$. Its corresponding complex-valued polynomial model parameters, which capture the AM/AM and AM/PM conversions, can be computed as in [33].

TABLE I

SIMULATION SETTINGS.

Description	**Value**	**Description**	**Value**
D (simulation area)	$1000 \times 1000m^2$	AP/UE distribution	ind. unif. rand.
Carrier frequency	2 GHz	AP/UE antenna height	$10/1.5$ m
Sbc bandwidth (Δf)	15 kHz	Coherence bandwidth	180 kHz
Coherence time	1 ms	τ_d (RUs)	168
ξ	0.5	σ_{sh}	4 dB
σ_b^2	-92 dBm	Bandwidth	15.36 MHz
$\eta_k^u \ \forall \ k$	100 mW	P_c	0.1 W
P_0	0.1 W	P_{bt}	0.25 W/(Gbits/s)

Finally, random pilot assignment is adopted for simplicity. So, each UE randomly select a pilot sequence from a predefined set of $\tau_p < K$ orthogonal pilot sequences of length τ_p samples.

B. Performance Evaluation

In order to evaluate the performance of the considered CF-mMIMO-OFDM system, we adopt the cumulative density function (CDF) of the SE, which corresponds to the SE values collected over different random realizations of the AP/UE locations for 500 network snapshots.

1) CF-mMIMO-OFDM Downlink under PA nonlinearity: Figs. 3(a) and 3(b) show the CDFs of the SEs achieved by the CF-mMIMO-OFDM adopting the *local* FZF precoding scheme and running under PA non-linearity. Both results achieved with ideal PA (black curve) and non-linear PA (with different values of IBO) are presented. First, one can observe that the results obtained in closed-form (solid curves) and by Monte-Carlo simulations (markers) are in good match, which numerically validates our derived closed-form expression in equation (34) for two L values (Fig. 3(a), $L = 200$ and Fig. 3(b), $L = 100$). Second, we can see the significant impact of the PA non-linearity on the SE performance, especially for high percentiles. The reason is that the PA distortion is beam-formed towards UEs with good channel conditions, since the control power scheme boosts the energy towards these UEs.

In Fig. 4, the CDFs of SEs achieved by the *local* RZF are given. It is worth noticing the higher sensitivity of the *local* RZF precoding scheme to the PA non-linearity compared to the FZF one. It is more clear now that only UEs with good channels (i.e., upper SE percentiles) are impacted.

In order to compare the impact of the non-linear PA on the performance of the two precoding schemes, *local* FZF and *local* RZF, Fig. 5 shows the CDFs of SEs when considering two values of IBO (6 and 9dB). Again, we can note that these latter suffer from the distortion caused by power amplifiers. Moreover, in linear case (Ideal PA), we observe that the RZF performs better than FZF, for low and high percentiles. The reason is that RZF can manage better the interference by taking into account channel estimation error and pilot contamination, thanks to the regularization matrix. Lastly, it is clear that RZF is more sensitive than FZF against the nonlinear distortions, especially at high SE percentiles. The reason is that the RZF boosts power towards UEs with good channel conditions, leading to high NLD power towards this UEs. Moreover, FZF still has worse performance at low SE percentiles because it

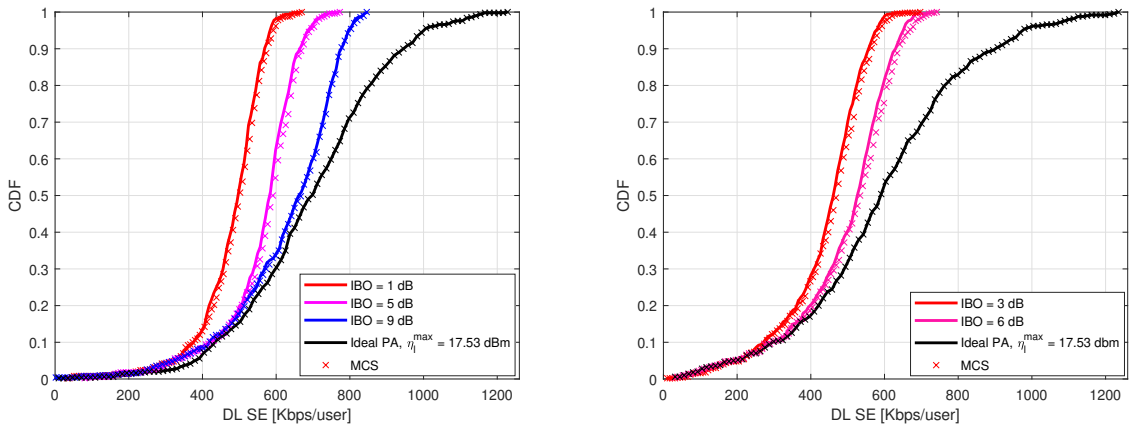

(a) $L = 200$ (b) $L = 100$

Fig. 3. CDFs of DL per-RB SE achieved by *local* FZF precoder: $M = 16$, $K = 20$, $\tau_p = 15$, power control is based on (13). Solid curves denote analytical results obtained in closed-form (equation (34)) while markers indicate the results obtained by MCS.

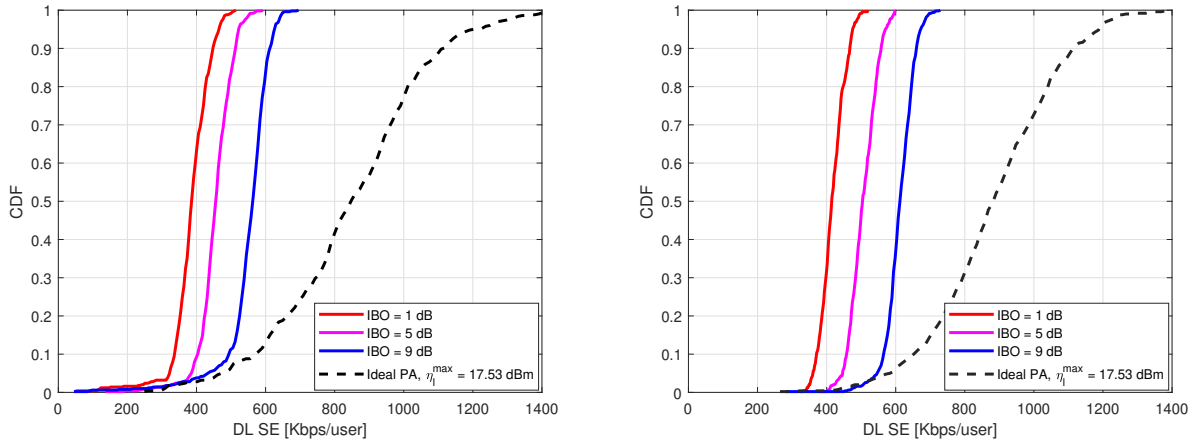

(a) $\tau_p = 15$ (b) $\tau_p = 20$

Fig. 4. CDFs of DL per-RB SE achieved by *local* RZF precoder: $L = 200$, $M = 16$, $K = 20$, power control is based on (13). Only results obtained by MCS are provided.

uses all the degrees of freedom to suppress interference towards all the available orthogonal directions, resulting in a small array gain $M - \tau_p$. By the way, it would be better to cancel only interference towards UEs ($< \tau_p$) with good channel gains and increase the array gain $M - \tau_p$.

Note that RZF can be improved by taking into account the NLD power in computing the regularization matrices $\{\mathbf{P}_l\}$, which is out of scope of this paper. The reason is because we aim to show the relevance of our proposed PAPR reduction algorithm in improving the performance of this traditional RZF.

2) Effect of the number of APs (L): Fig. 6 illustrates the median per-RB SE, averaged over many large-scale fading realizations, versus the number of APs (L). Both results obtained in closed-form and by MCSs are given for *local* FZF precoding schemes. One can first observe the good match between theoretical ans simulation results

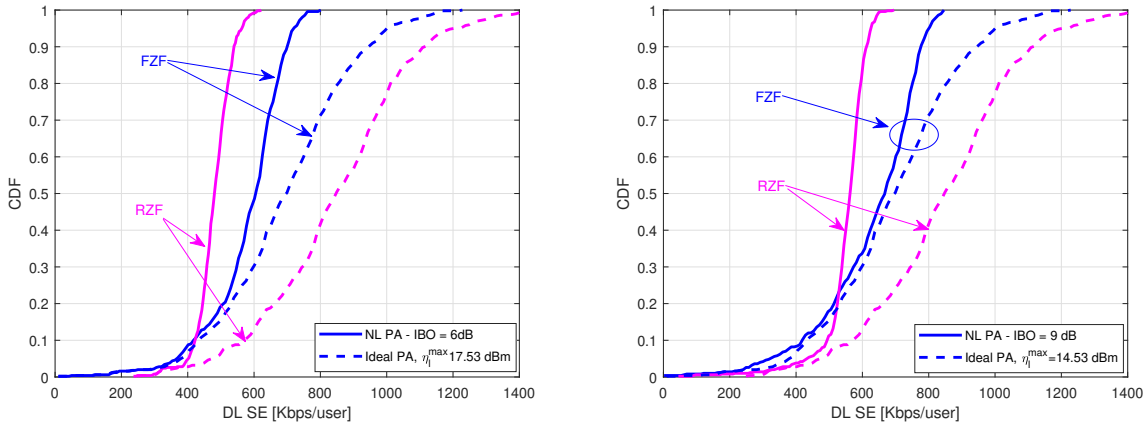

(a) IBO = 6dB (b) IBO = 9dB

Fig. 5. CDFs of DL per-RB SE achieved by FZF and RZF precoders: $L = 200$, $M = 16$, $K = 20$, $\tau_p = 15$, power control is based on (13).

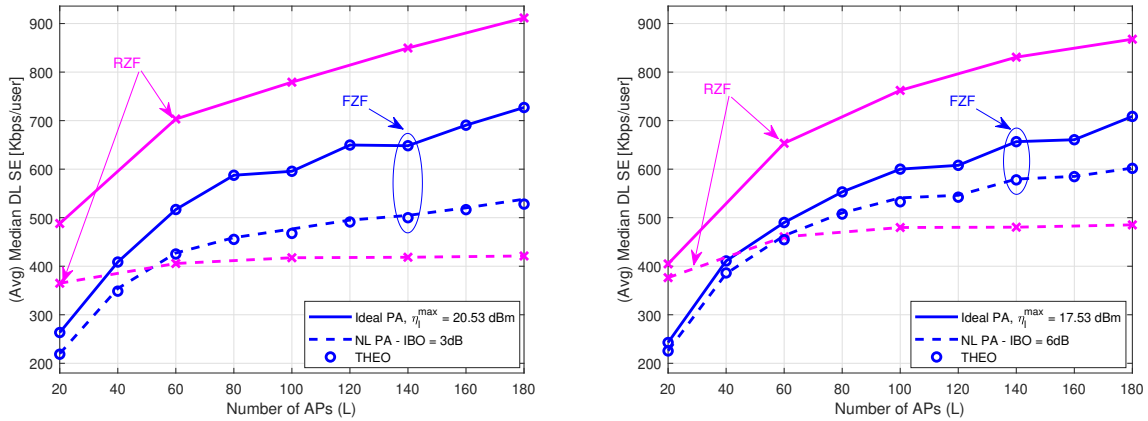

(a) IBO = 3dB (b) IBO = 6dB

Fig. 6. Median DL per-RB SE, achieved by FZF and RZF precoders, averaged over several large-scale fading realizations, $M = 16$, $K = 20$, $\tau_p = 15$. Solid curves denote results obtained by MCS while circle markers indicate the results obtained in closed-form (equation (34) for FZF.

for the different values of L, validating our derived analytical expression in (34). From these results, it is clear that the SE of the system impacted by PA is degraded w.r.t. the system with ideal PA. Again, we can note the higher sensitivity of the RZF against the nonlinear distortions compared to FZF, which is as more pronounced as the number of APs increases. It is worth mentioning that, with FZF, the DL SE performance does not tend to an upper bound at large L, while, with RZF, the DL SE performance is upper bounded.

Lastly, from results depicted in Fig. 7, one can see that the DL SE loss, caused by power amplifiers, gets larger when the number of APs gets higher. For an $IBO = 3$, the FZF-related SE loss gets higher from 17.32% to 25.98% when the number of APs grows from 60 to 180. While the SE loss achieved by the RZF increases from 45.55% to 56.51%.

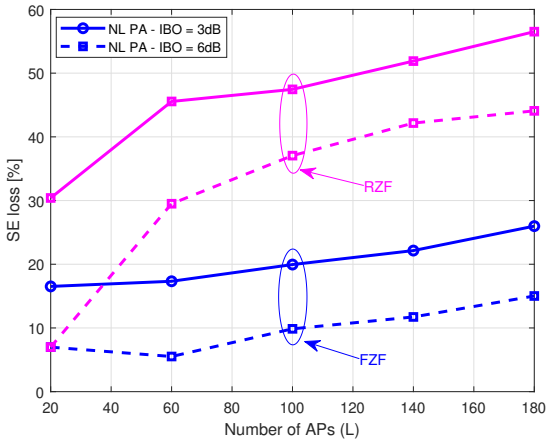

Fig. 7. DL SE loss caused by nonlinear distortion on FZF and RZF precoders, averaged over several large-scale fading realizations, $M = 16$, $K = 20$, $\tau_p = 15$.

3) Effect of the number of pilots (τ_p): The implementation versatility of RZF versus the limitation of FZF is shown in Fig. 8. When M is fixed, RZF precoding can be performed by any number of pilots τ_p, while FZF constraints the number of orthogonal pilots, such that $\tau_p < M$ has to be verified (else the FZF inverse peudo-matrix is not defined). For instance, Figs. 8(a) and 8(b) show the ability of RZF to achieve much higher SEs in the operation regime in which FZF cannot be implemented. Moreover, we can observe from these results a loss in the performance of the FZF when τ_p goes from 12 to 15. In linear case, it gets lower from 4.68 to 3.99 kbps/user. Such degradation is caused by decreasing the array gain $M - \tau_p$ when τ_p tends to M. This confirm the intuition saying to only cancel interference towards UEs ($< \tau_p$) with good channel gains, leading to increase the array gain $M - \tau_p$. In nonlinear case, FZF performs better than RZF in its implementable operation regime, else it does not. For $\tau_p = 12$, FZF has a gain of 60% and 57% for, respectively, an IBO of 6dB and 3dB.

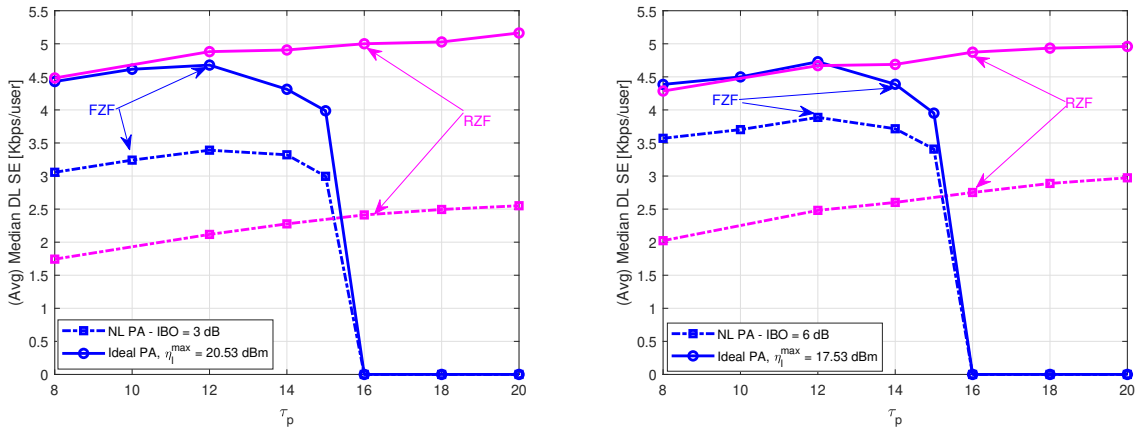

(a) IBO = 3dB (b) IBO = 6dB

Fig. 8. Median DL per-RB SE, achieved by FZF and RZF precoders, averaged over several large-scale fading realizations, $M = 16$, $K = 20$, $\tau_p = 15$. Only results obtained by MCS are provided.

4) PAPR reduction: To evaluate the efficiency of the proposed *local*PAPR*free* algorithm in terms of PAPR reduction, we adopt the complementary cumulative distribution function (CCDF) to evaluate the PAPR reduction performance. The CCDF denotes the probability that the PAPR of the transmitted signal is higher than a given threshold PAPR0.

In Figs. 9(a) and 9(b), we show the CCDF of the PAPR for, respectively, FZF and RZF, when different numbers of iterations are considered. Note that PAPRs associated with all the antennas of all the APs are taken into account in computing the empirical CCDF. The number of trials is chosen to be 5000 in our simulations. Looking at these results, one can clearly note that the *local*PAPR*free* algorithm offers substantial PAPR reduction compared with the original *local* FZF and RZF precoding schemes. Indeed, for the FZF, it achieves a gain of 3.09dB, 4.94dB and 5.71dB when, respectively, 1, 3 and 5 iterations are considered (at a CCDF of 1%). That is really obvious that it converges so fast, thanks to the regularization factor ν_l computed in equation (47).

In order to see the impact of τ_p and τ_s on the PAPR performance, we plot in 9(a) results achieved when considering FZF with $\tau_p = 15$ and $\tau_s = 8$ and in 9(b) results achieved when considering RZF with $\tau_p = 20$ and $\tau_s = 10$. One can see a slight better performance when τ_s is larger, i.e. the projection space is larger. It is worth to mention that these values of τ_s have chosen empirically, such that we have the best PAPR reduction without damaging the transmission quality.

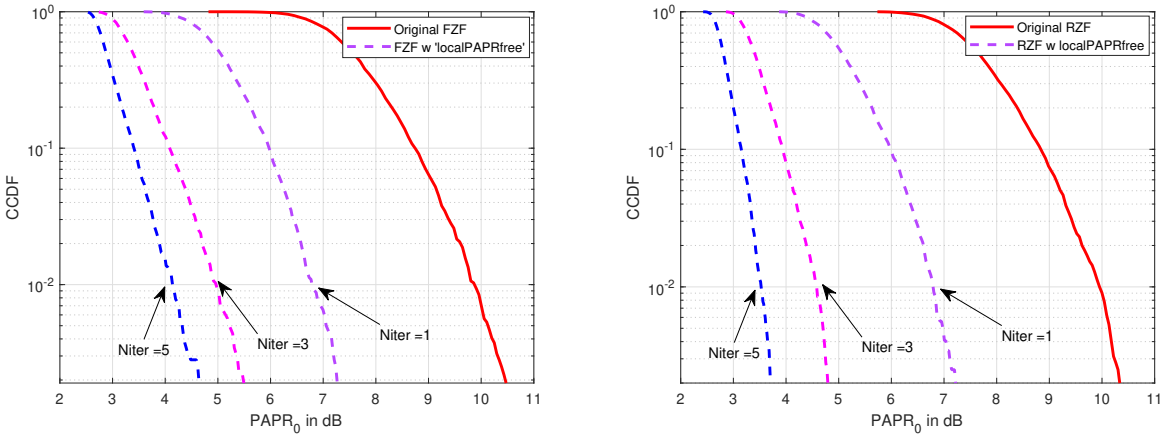

(a) FZF, $\tau_p = 15$, $\tau_s = 8$ (b) RZF, $\tau_p = 20$, $\tau_s = 10$

Fig. 9. CCDFs of PAPR: $L = 200$, $M = 16$, $K = 20$, power control is based on 13.

We recall that the *local*PAPR*free* algorithm can be applied in a distributed and scalable fashion, i.e., implemented at each AP and executed locally, making benefits of scalable and high energy-efficient CF-mMIMO-OFDM.

In addition to the performance in terms of PAPR reduction, it is important to study the impact of the developed algorithm on the DL SE. To clearly see the impact of the PAPR reduction, we assume that the power amplifiers are perfectly linearized, i.e, a perfect digital predistortion (DPD) is added before each PA [41][42]. Then, this latter acts as a limiter.

To this end, Figs. 10 and 11 show the CDFs of the SEs achieved by the CF-mMIMO-OFDM adopting, respectively, the FZF and RZF precoding schemes. Results achieved with or without the *local*PAPR*free* algorithm are provided.

We recall that the user grouping, related to the PAPR reduction, is based on the user path-loss: the τ_s users having the highest path-losses belong to Ω_l (set of strong users), while $\tau_p - \tau_s$ users belong to Ω_l^c (set of weak users). It is worth mentioning that if UE $k \in \Omega_l$, any UE $t \in \mathcal{P}_k$ belongs to Ω_l, such that the users using the same pilot undergoes that same effect. In this comparison, the simulation setup consists in $L = 200$, $M = 16$, $K = 20$. For

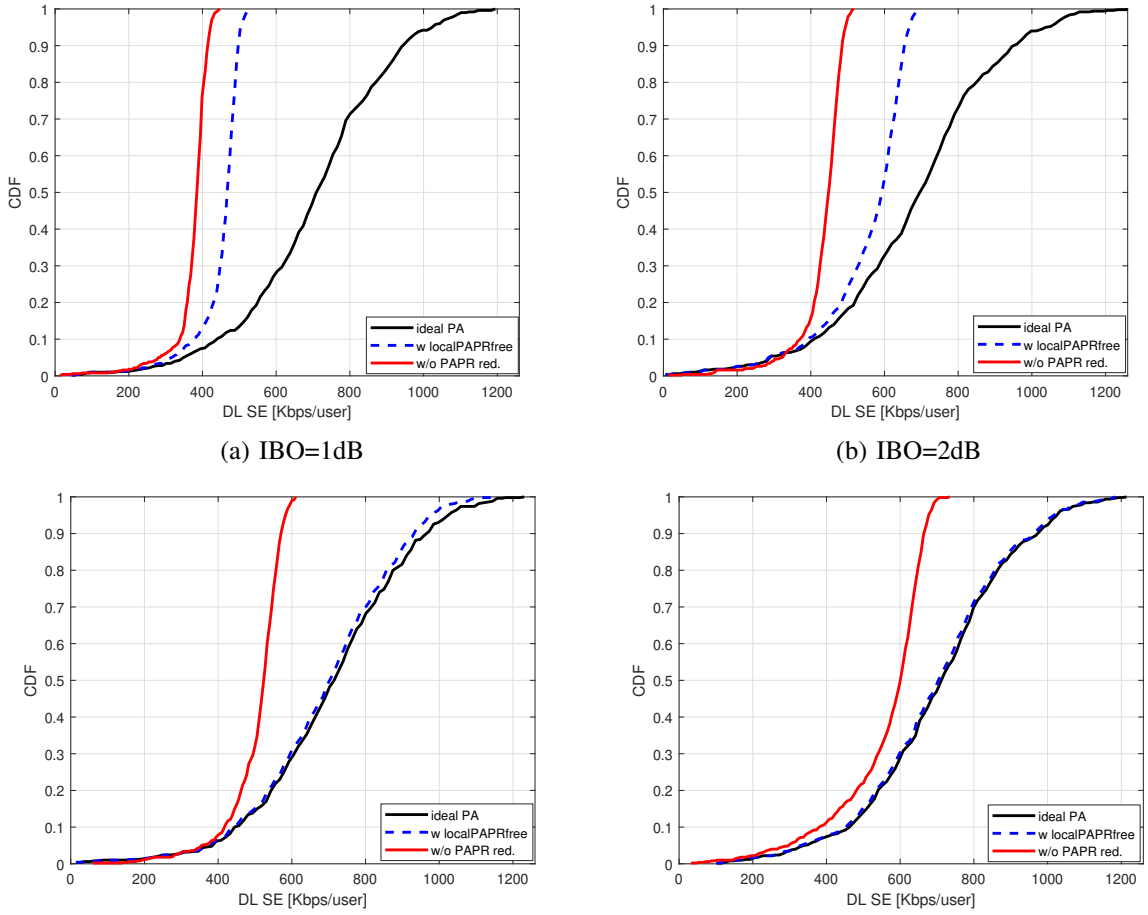

(a) IBO=1dB (b) IBO=2dB

(c) IBO=3dB (d) IBO=4dB

Fig. 10. CDFs of DL per-RB SE achieved FZF precoders: $L = 200$, $M = 16$, $K = 20$, $\tau_p = 15$, $\tau_s = 8$, power control is based on (13).

FZF, $\tau_p = 15$, $\tau_s = 8$, while $\tau_p = 20$, $\tau_s = 10$ for RZF. Here, the results achieved by the use of the *local*PAPR*free* algorithm (dashed blue curves) corresponds to PAPR performance, given in Figs. 10 and 11, with $Niter = 5$. We can clearly observe the robustness of the proposed PAPR-aware precoding scheme against the saturation effects compared to the traditional *local* FZF and RZF precoding schemes (red curves). With the proposed scheme, we can achieve the same DL SE as with ideal PAs (benchmark, black curves) from an IBO of 3dB. Moreover, it performs better than the case without PAPR reduction when the PAs are operated with lower IBO values (1 and 2dB). Most importantly, although the sensitivity of RZF against PA-related NLD, it caches up and gains in performance (see Fig. 11).

When coming to Figs. 12(a) and 12(b) other comments can be highlighted. Indeed, we can clearly see the ability of the *local*PAPR*free* algorithm to enhance the median DL SE. The maximum gain is achieved when the IBO is

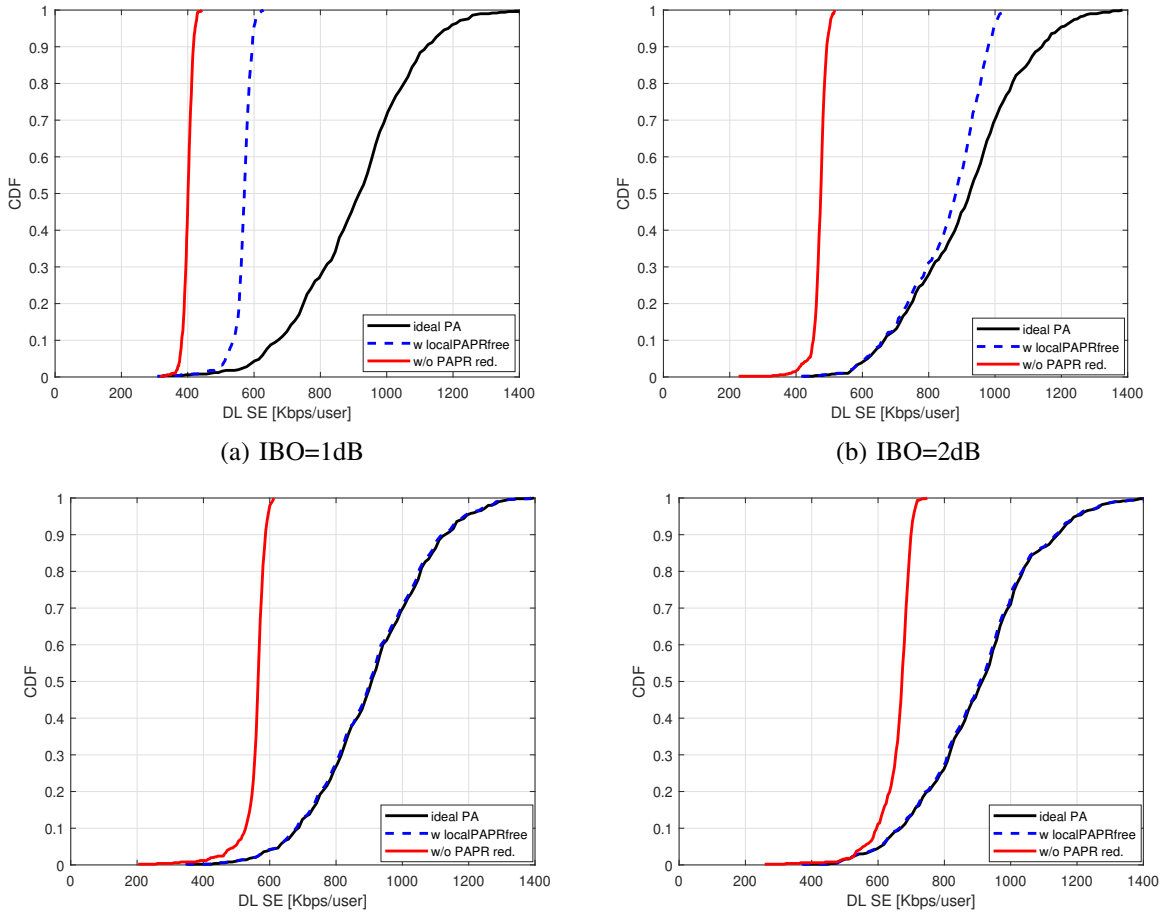

(a) IBO=1dB (b) IBO=2dB

(c) IBO=3dB (d) IBO=4dB

Fig. 11. CDFs of DL per-RB SE achieved RZF precoders: $L = 200$, $M = 16$, $K = 20$, $\tau_p = 20$, $\tau_s = 10$, power control is based on (13).

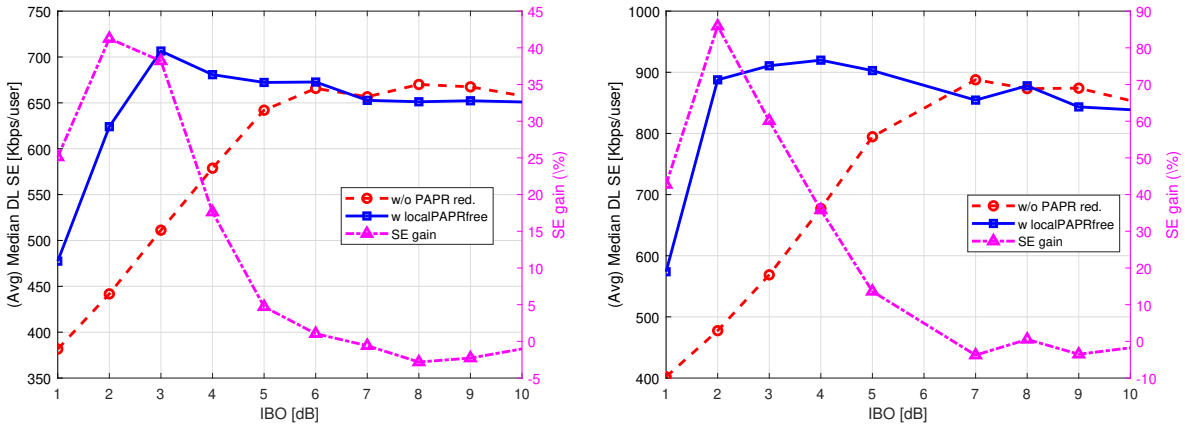

(a) FZF with $\tau_p = 15$, $\tau_s = 8$ (b) RZF with $\tau_p = 20$, $\tau_s = 10$

Fig. 12. Median DL per-RB SE achieved by FZF and RZF precoding schemes, averaged over several large-scale fading realizations, $L = 200$, $M = 16$, $K = 20$.

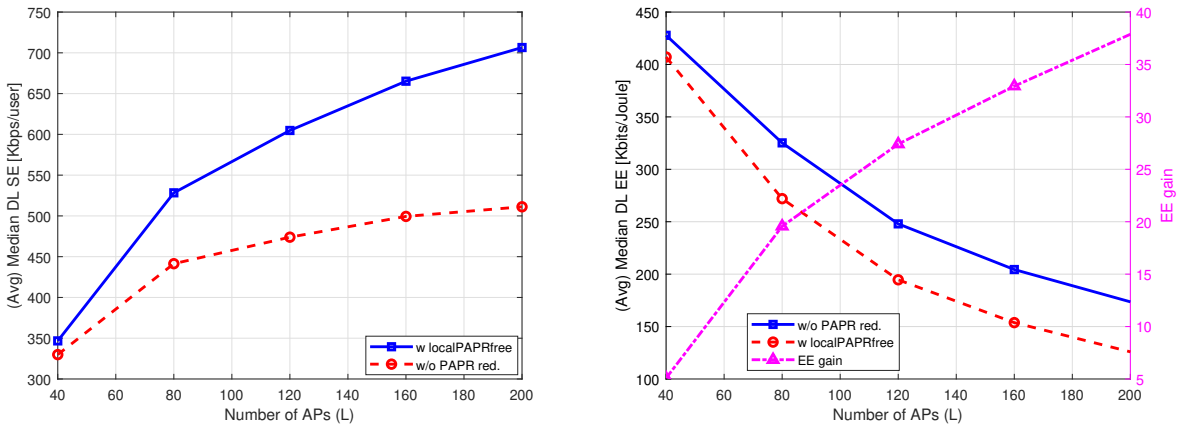

(a) DL SE (b) DL EE

Fig. 13. Median DL per-RB SE and EE versus the number of APs, achieved by FZF precoding scheme, averaged over several large-scale fading realizations, $M = 16$, $K = 20$, $\tau_p = 15$, $\tau_s = 8$, IBO $= 3$dB, $\eta_l^{max} = 20.53$dBm.

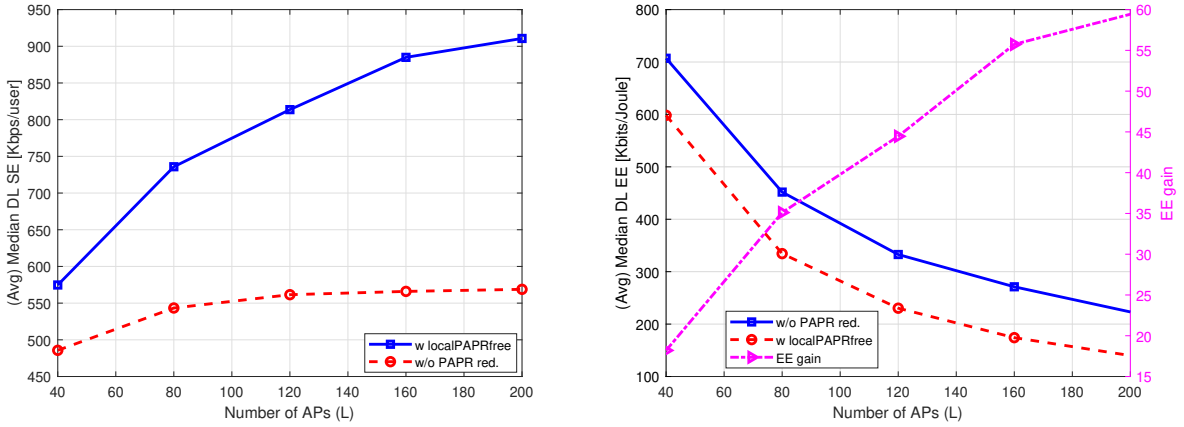

(a) DL SE (b) DL EE

Fig. 14. Median DL per-RB SE and EE versus the number of APs, achieved by RZF precoding scheme, averaged over several large-scale fading realizations, $M = 16$, $K = 20$, $\tau_p = 20$, $\tau_s = 10$, IBO $= 3$dB, $\eta_l^{max} = 20.53$dBm.

equal to 2dB, it is about 41% and 86% for, respectively, FZF and RZF.

To further evaluate the effectiveness of the proposed *local*PAPR*free* algorithm, we compare the average spectral efficiency and energy efficiency of our PAPR reduction method with the classical *local* FZF and RZF precoding schemes without any PAPR reuction (see Figs. 13 and 14). Moreover, the gain in terms of energy efficiency is also given versus the number of APs and the IBO is equal to 3dB. Looking at these results, with our proposed PAPR reuction method, the DL SE and EE improve significantly. In particular, the provided gain increases while the number of APs (L) is increasing. When L varies from 100 to 200, it goes from 23% to 38% and from 40% to 60% for, respectively, FZF and RZF (as shown by Figs. 13(b) and **??**(b)).

TABLE II
OOB [dB] RADIATION PERFORMANCE.

IBO [dB]	**1**	**3**	**6**	**9**	**12**
FZF/RZF w/o PAPR red.	-10.92	-14.86	-25.46	-46.49	-301.5
FZF/RZF w *local*PAPR*free* ($\tau_p = 15$, $\tau_s = 8$)	-17.77	-41.45	-304	-304	-304
RZF w *local*PAPR*free* ($\tau_p = 20$, $\tau_s = 10$)	-20.14	-297.21	-304	-304	-304

C. Out-of-band (OOB) radiation performance

In order to measure the amount of signal power that is transmitted outside the active subcarriers Ξ, we define the OOB radiation as follows

$$\text{OOB [dB]} = 10\log_{10}\left(\frac{\sum_{n\in\Xi^c}\|\mathbf{x}_n\|_2^2}{\sum_{n\in\Xi}\|\mathbf{x}_n\|_2^2}\right) \tag{50}$$

Note that for FZF and RZF precoding schemes, we have OOB $= -\infty$ (dB), as no data is transmitted over the guard-band. Nevertheless, we have OOB > 0 in presence of non-linear power amplifiers. Interestingly, the proposed *local*PAPR*free* algorithm does not ignore the OOB radiation and it ensures that the signal power on subcarriers Ξ^c is zero, such that no interference is caused by the PAPR reduction, in the guard-band (the constraint on the OOB is given in the algorithm's Step 8, as shown in Table **Algorithm**). Table II gives the OOB radiation performance of the proposed algorithm compared to the classical FZF/RZF without any PAPR reduction, with PAs acting as limiters operating at IBO of 1, 3, 6, 9 and 12. One can clearly note that the *local*PAPR*free* algorithm can perform satisfactory OOB radiation performance from an IBO of $3dB$ (OOB radiation $< -41dB$), making our solution useful in practice.

VI. CONCLUSION

The proposed *local*PAPR*free* algorithm is a versatile distributed PAPR reduction method that can significantly reduce the PAPR of transmitted signals and then improve spectral efficiency and the energy efficiency of an OFDM based cell-free massive MIMO system, compared to the traditional precoding schemes. Specifically, the *local*PAPR*free* algorithm can anticipate the PA related distortions and adds frequency domain peak-cancelling signals to the transmitted ones (generated by the traditional precoding scheme), reducing the PAPR and avoiding the PA distortions. Interestingly, the *local*PAPR*free* can, via the added PCSs, control the radiated distortion. This latter is optimized such that it is negligible towards the UEs with good channel gains while it can be tolerable towards UEs with poor channel gains. Indeed, it is not necessary to cancel distortion towards all the available directions, a finding that have have shown through the theoretical study conducted within this investigation. Moreover, we have shown that the DL SE increases unlimitedly as number of APs grows while a SE loss is increasing compared to the linear case.

It is worth mentioning that the application of the proposed algorithm with the other existing *local* precoding schemes (like *local* partial ZF and *local* protective partial ZF [11]) is straightforward, certainly constitutes an

intended future work. In addition, improving the EE analysis through the use of realistic power consumption models for power amplifiers and back-hauling is of paramount importance.

APPENDIX A

From equation (29), we need first to compute $\left|\sum_{l=1}^{L}\sqrt{\eta_{l,k}}\mathrm{E}\left\{\mathbf{h}_{l,k,n}^{H}\mathbf{K}_0\mathbf{w}_{l,n,i_k}\right\}\right|^2$, $\mathrm{E}\left\{|\mathrm{PGU}_{k,n}|^2\right\}$ and $\sum_{t\neq k}^{K}\mathrm{E}\left\{|\mathrm{MUI}_{kt,n}|^2\right\}$.

$$\begin{aligned}\left|\sum_{l=1}^{L}\sqrt{\eta_{l,k}}\mathrm{E}\left\{\mathbf{h}_{l,k,n}^{H}\mathbf{K}_0\mathbf{w}_{l,n,i_k}\right\}\right|^2 &\overset{(a)}{=} |K_0|^2\left(\sum_{l=1}^{L}\sqrt{\eta_{l,k}}\alpha_{l,k,k}\right)^2 \\ &\overset{(b)}{=} (M-\tau_p)|K_0|^2\left(\sum_{l=1}^{L}\sqrt{\eta_{l,k}\gamma_{l,k}}\right)^2, \text{ for FZF}\end{aligned} \tag{51}$$

where:

- in (a) the diagonal matrix $\mathbf{K}_0$ whose elements are equal to the complex coefficient K_0 as we assume the adoption of the same power amplifier at each antenna branch of each AP.
- in (b) $\alpha_{l,k,k}$ is equal to $\sqrt{(M-\tau_p)\gamma_{l,k}}$ for FZF precoding scheme as explained in [11].

Next, we compute $\sum_{t=1}^{K}\mathrm{E}\left\{\left|\sum_{l=1}^{L}\sqrt{\eta_{l,t}}\mathbf{h}_{l,k,n}^{H}\mathbf{K}_0\mathbf{w}_{l,n,i_t}\right|^2\right\}$.

$$\begin{aligned}&\sum_{t=1}^{K}\mathrm{E}\left\{\left|\sum_{l=1}^{L}\sqrt{\eta_{l,t}}\mathbf{h}_{l,k,n}^{H}\mathbf{K}_0\mathbf{w}_{l,n,i_t}\right|^2\right\} \\ &= \sum_{t=1}^{K}\mathrm{E}\left\{\left|\sum_{l=1}^{L}|K_0|\sqrt{\eta_{l,t}}\left(\hat{\mathbf{h}}_{l,k,n}^{H}\mathbf{w}_{l,n,i_t}+\tilde{\mathbf{h}}_{l,k,n}^{H}\mathbf{w}_{l,n,i_t}\right)\right|^2\right\} \\ &= \sum_{t=1}^{K}\sum_{l=1}^{L}\sum_{l\prime=1}^{L}|K_0|^2\sqrt{\eta_{l,t}\eta_{l\prime,t}}\left(\alpha_{l,k,t}\alpha_{l\prime,k,t}+\mathrm{E}\left\{\tilde{\mathbf{h}}_{l,k,n}^{H}\mathbf{w}_{l,n,i_t}\mathbf{w}_{l\prime,n,i_t}^{H}\tilde{\mathbf{h}}_{l\prime,k,n}\right\}\right) \\ &\overset{(c)}{=} (M-\tau_p)|K_0|^2\sum_{t\in\mathcal{P}_k}\left(\sum_{l=1}^{L}\sqrt{\eta_{l,t}\gamma_{l,k}}\right)^2+|K_0|^2\sum_{t=1}^{K}\sum_{l=1}^{L}\eta_{l,t}(\beta_{l,k}-\gamma_{l,k}), \text{ for FZF}\end{aligned} \tag{52}$$

for more details concerning (c), the reader can refer to [11][36].

The NLD variance $\Psi_{k,n}$ can be approximated as

$$\begin{aligned}
\Psi_{k,n} &= \mathrm{E}\left\{ |\sum_{l=1}^{L} \mathbf{h}_{l,k,n}^{H} \mathbf{d}_{l,n}|^2 \right\} \qquad (53)\\
&= \sum_{l=1}^{L}\sum_{l\prime=1}^{L} \mathrm{E}\left\{ \mathbf{h}_{l,k,n}^{H} \mathbf{d}_{l,n} \mathbf{d}_{l\prime,n}^{H} \mathbf{h}_{l\prime,k,n} \right\} \\
&= \sum_{l=1}^{L}\sum_{l\prime=1}^{L} \mathrm{E}\left\{ \left(\sum_{m=1}^{M} h_{l,k,n,m}^{*} d_{l,n,m} \right) \left(\sum_{m\prime=1}^{M} d_{l\prime,n,m\prime}^{*} h_{l\prime,k,n,m\prime} \right) \right\} \\
&= \sum_{l=1}^{L}\sum_{l\prime=1}^{L}\sum_{m=1}^{M}\sum_{m\prime=1}^{M} \mathrm{E}\left\{ h_{l,k,n,m}^{*} d_{l,n,m} d_{l\prime,n,m\prime}^{*} h_{l\prime,k,n,m\prime} \right\} \\
&\overset{(d)}{=} \sum_{l=1}^{L}\sum_{m=1}^{M} \mathrm{E}\left\{ h_{l,k,n,m}^{*} d_{l,n,m} d_{l,n,m}^{*} h_{l,k,n,m} \right\} + \sum_{l=1}^{L}\sum_{l\prime\neq l}^{L}\sum_{m=1}^{M}\sum_{m\prime\neq m}^{M} \mathrm{E}\left\{ h_{l,k,n,m}^{*} d_{l,n,m} d_{l\prime,n,m\prime}^{*} h_{l\prime,k,n,m\prime} \right\} \\
&\overset{(e)}{=} \sum_{l=1}^{L}\sum_{m=1}^{M} \mathrm{E}\left\{ h_{l,k,n,m}^{*} \sigma_d^2 h_{l,k,n,m} \right\} + \sum_{l=1}^{L}\sum_{l\prime\neq l}^{L}\sum_{m=1}^{M}\sum_{m\prime\neq m}^{M} \mathrm{E}\left\{ h_{l,k,n,m}^{*} \sigma_d^{2(\prime)} h_{l\prime,k,n,m\prime} \right\} \\
&\overset{(f)}{=} M \sum_{l=1}^{L} \beta_{l,k} \sigma_d^2
\end{aligned}$$

The two terms in (d) represents, respectively, the intra-AP and inter-AP distortions. The cross term can be neglected since channels are uncorrelated to the distortion noise. The first term in (d) contains inter-user and intra-user interference. (e) is obtained by assuming that the channel is constant during a time-interval (channel coherence time). In (e), the average distortion power can be approximated only by intra-user interference since the *local* FZF precoding scheme is able to considerably reduce the inter-user interference, when $\tau_p \to M$. Therefore, (e) can be resumed in (f). Normalizing (e) w.r.t. to the noise power σ_b^2, we find equation (33).

Plugging 51, 52 and 53 into 29 gives 34.

REFERENCES

[1] I. Hwang, B. Song, and S. S. Soliman, "A holistic view on hyper-dense heterogeneous and small cell networks," *IEEE Communications Magazine*, vol. 51, no. 6, pp. 20–27, 2013.

[2] D. López-Pérez, M. Ding, H. Claussen, and A. H. Jafari, "Towards 1 gbps/ue in cellular systems: Understanding ultra-dense small cell deployments," *IEEE Communications Surveys Tutorials*, vol. 17, no. 4, pp. 2078–2101, 2015.

[3] T. L. Marzetta, "Noncooperative cellular wireless with unlimited numbers of base station antennas," *IEEE Transactions on Wireless Communications*, vol. 9, no. 11, pp. 3590–3600, 2010.

[4] E. Björnson, J. Hoydis, and L. Sanguinetti, *Massive MIMO Networks: Spectral, Energy, and Hardware Efficiency*. Now Foundations and Trends, 2017.

[5] H. Q. Ngo, A. Ashikhmin, H. Yang, E. G. Larsson, and T. L. Marzetta, "Cell-free massive mimo versus small cells," *IEEE Transactions on Wireless Communications*, vol. 16, no. 3, pp. 1834–1850, 2017.

[6] S. Venkatesan, A. Lozano, and R. Valenzuela, "Network mimo: Overcoming intercell interference in indoor wireless systems," in *2007 Conference Record of the Forty-First Asilomar Conference on Signals, Systems and Computers*, 2007, pp. 83–87.

[7] X.-H. You, D.-M. Wang, B. Sheng, X.-Q. Gao, X.-S. Zhao, and M. Chen, "Cooperative distributed antenna systems for mobile communications [coordinated and distributed mimo]," *IEEE Wireless Communications*, vol. 17, no. 3, pp. 35–43, 2010.

[8] S. Zhou, M. Zhao, X. Xu, J. Wang, and Y. Yao, "Distributed wireless communication system: a new architecture for future public wireless access," *IEEE Communications Magazine*, vol. 41, no. 3, pp. 108–113, 2003.

[9] R. Irmer, H. Droste, P. Marsch, M. Grieger, G. Fettweis, S. Brueck, H.-P. Mayer, L. Thiele, and V. Jungnickel, "Coordinated multipoint: Concepts, performance, and field trial results," *IEEE Communications Magazine*, vol. 49, no. 2, pp. 102–111, 2011.

[10] E. Björnson and L. Sanguinetti, "Scalable cell-free massive mimo systems," *IEEE Transactions on Communications*, vol. 68, no. 7, pp. 4247–4261, 2020.

[11] G. Interdonato, M. Karlsson, E. Björnson, and E. G. Larsson, "Local partial zero-forcing precoding for cell-free massive mimo," *IEEE Transactions on Wireless Communications*, vol. 19, no. 7, pp. 4758–4774, 2020.

[12] J. Zhang, J. Zhang, E. Björnson, and B. Ai, "Local partial zero-forcing combining for cell-free massive mimo systems," *IEEE Transactions on Communications*, vol. 69, no. 12, pp. 8459–8473, 2021.

[13] D. Wulich and L. Goldfeld, "Reduction of peak factor in orthogonal multicarrier modulation by amplitude limiting and coding," *IEEE Transactions on Communications*, vol. 47, no. 1, pp. 18–21, 1999.

[14] H. Li, T. Jiang, and Y. Zhou, "An improved tone reservation scheme with fast convergence for papr reduction in ofdm systems," *IEEE Transactions on Broadcasting*, vol. 57, no. 4, pp. 902–906, 2011.

[15] S. K. Chaitanya Bulusu, H. Shaiek, D. Roviras, and R. Zayani, "Reduction of papr for fbmc-oqam systems using dispersive slm technique," in *2014 11th International Symposium on Wireless Communications Systems (ISWCS)*, 2014, pp. 568–572.

[16] J.-C. Chen, "Partial transmit sequences for peak-to-average power ratio reduction of ofdm signals with the cross-entropy method," *IEEE Signal Processing Letters*, vol. 16, no. 6, pp. 545–548, 2009.

[17] S.-H. Wang, W.-L. Lin, B.-R. Huang, and C.-P. Li, "Papr reduction in ofdm systems using active constellation extension and subcarrier grouping techniques," *IEEE Communications Letters*, vol. 20, no. 12, pp. 2378–2381, 2016.

[18] S. Shu, D. Qu, L. Li, and T. Jiang, "Invertible subset qc-ldpc codes for papr reduction of ofdm signals," *IEEE Transactions on Broadcasting*, vol. 61, no. 2, pp. 290–298, 2015.

[19] K. Anoh, C. Tanriover, and B. Adebisi, "On the optimization of iterative clipping and filtering for papr reduction in ofdm systems," *IEEE Access*, vol. 5, pp. 12 004–12 013, 2017.

[20] C. Studer and E. G. Larsson, "Par-aware large-scale multi-user mimo-ofdm downlink," *IEEE Journal on Selected Areas in Communications*, vol. 31, no. 2, pp. 303–313, 2013.

[21] H. Bao, J. Fang, Z. Chen, H. Li, and S. Li, "An efficient bayesian papr reduction method for ofdm-based massive mimo systems," *IEEE Transactions on Wireless Communications*, vol. 15, no. 6, pp. 4183–4195, 2016.

[22] H. Bao, J. Fang, Q. Wan, Z. Chen, and T. Jiang, "An admm approach for papr reduction for large-scale mimo-ofdm systems," *IEEE Transactions on Vehicular Technology*, vol. 67, no. 8, pp. 7407–7418, 2018.

[23] R. Zayani, H. Shaiek, and D. Roviras, "PAPR-Aware Massive MIMO-OFDM Downlink," *IEEE Access*, vol. 7, pp. 25 474–25 484, 2019.

[24] R. Zayani and D. Roviras, "Low-complexity linear precoding for low-papr massive mu-mimo-ofdm downlink systems," *International Journal of Communication Systems*, 2021.

[25] G. Interdonato, M. Karlsson, E. Bjornson, and E. G. Larsson, "Downlink spectral efficiency of cell-free massive mimo with full-pilot zero-forcing," in *2018 IEEE Global Conference on Signal and Information Processing (GlobalSIP)*, 2018, pp. 1003–1007.

[26] W. Jiang and H. D. Schotten, "Cell-free massive mimo-ofdm transmission over frequency-selective fading channels," *IEEE Communications Letters*, vol. 25, no. 8, pp. 2718–2722, 2021.

[27] Z. Mokhtari and R. Dinis, "Sum-rate of cell free massive mimo systems with power amplifier non-linearity," *IEEE Access*, vol. 9, pp. 141 927–141 937, 2021.

[28] A. K. Papazafeiropoulos, E. Björnson, P. Kourtessis, S. Chatzinotas, and J. M. Senior, "Scalable cell-free massive mimo systems with hardware impairments," in *2020 IEEE 31st Annual International Symposium on Personal, Indoor and Mobile Radio Communications*, 2020, pp. 1–7.

[29] J. Vieira, F. Rusek, O. Edfors, S. Malkowsky, L. Liu, and F. Tufvesson, "Reciprocity calibration for massive mimo: Proposal, modeling, and validation," *IEEE Transactions on Wireless Communications*, vol. 16, no. 5, pp. 3042–3056, 2017.

[30] W. Zeng, Y. He, B. Li, and S. Wang, "Pilot assignment for cell free massive mimo systems using a weighted graphic framework," *IEEE Transactions on Vehicular Technology*, vol. 70, no. 6, pp. 6190–6194, 2021.

[31] S. M. Kay, *Fundamentals of Statistical Signal Processing: Estimation Theory*. USA: Prentice-Hall, Inc., 1993.

[32] R. Price, "A useful theorem for nonlinear devices having gaussian inputs," *IRE Transactions on Information Theory*, vol. 4, no. 2, pp. 69–72, 1958.

[33] M. C. Dakhli, R. Zayani, O. B. Belkacem, and R. Bouallegue, "Theoretical analysis and compensation for the joint effects of hpa nonlinearity and rf crosstalk in vblast mimo-ofdm systems over rayleigh fading channel," *Eurasip Journal on Wireless Communications and Networking*, vol. 2014, no. 61, 214.

[34] H. Shaiek, R. Zayani, Y. Medjahdi, and D. Roviras, "Analytical analysis of ser for beyond 5g post-ofdm waveforms in presence of high power amplifiers," *IEEE Access*, vol. 7, pp. 29 441–29 452, 2019.

[35] M. T. L., E. G. Larsson, H. Yang, and H. Q. Ngo, *Fundamentals of Massive MIMO*. U.K.: Cambridge, U.K.: Cambridge Univ. Press, 2016.

[36] H. Q. Ngo, L.-N. Tran, T. Q. Duong, M. Matthaiou, and E. G. Larsson, "On the total energy efficiency of cell-free massive mimo," *IEEE Transactions on Green Communications and Networking*, vol. 2, no. 1, pp. 25–39, 2018.

[37] B. Dai and W. Yu, "Energy efficiency of downlink transmission strategies for cloud radio access networks," *IEEE Journal on Selected Areas in Communications*, vol. 34, no. 4, pp. 1037–1050, 2016.

[38] E. Björnson, L. Sanguinetti, J. Hoydis, and M. Debbah, "Optimal design of energy-efficient multi-user mimo systems: Is massive mimo the answer?" *IEEE Transactions on Wireless Communications*, vol. 14, no. 6, pp. 3059–3075, 2015.

[39] "Further advancements for e-utra physical layer aspects (release 9)," *3GPP, document TS 36.814, Mar. 2017*, 2017.

[40] Nokia, "Realistic power amplifier model for the new radio evaluation," *document R4-163314, 3GPP TSG-RAN WG4 Meeting 79*, 2016.

[41] R. Zayani, R. Bouallegue, and D. Roviras, "Adaptive predistortions based on neural networks associated with levenberg-marquardt algorithm for satellite down links," *EURASIP Journal on Wireless Communications and Networking*, pp. 1687–1499, 2008.

[42] A. Falempin, R. Zayani, J.-B. Doré, and E. C. Strinati, "Low-complexity adaptive digital pre-distortion with meta-learning based neural networks," in *2022 IEEE 19th Annual Consumer Communications Networking Conference (CCNC)*, 2022, pp. 453–453.